Title

Maize death acids, 9-lipoxygenase–derived cyclopente(a)nones, display activity as cytotoxic phytoalexins and transcriptional mediators

Journal

Proceedings of the National Academy of Sciences of the United States of America, 112(36)

ISSN

0027-8424

Authors

Christensen, Shawn A
Huffaker, Alisa
Kaplan, Fatma
et al.

Publication Date

2015-09-08

DOI

10.1073/pnas.1511131112

Peer reviewed

Maize death acids, 9-lipoxygenase–derived cyclopente(a)nones, display activity as cytotoxic phytoalexins and transcriptional mediators

Shawn A. Christensen[a], Alisa Huffaker[b], Fatma Kaplan[c], James Sims[d], Sebastian Ziemann[e], Gunther Doehlemann[e], Lexiang Ji[f], Robert J. Schmitz[g], Michael V. Kolomiets[h], Hans T. Alborn[a], Naoki Mori[i], Georg Jander[j], Xinzhi Ni[k], Ryan C. Sartor[b], Sara Byers[l], Zaid Abdo[l], and Eric A. Schmelz[b,1]

[a]Chemistry Research Unit, Center for Medical, Agricultural, and Veterinary Entomology, Department of Agriculture–Agricultural Research Service (USDA–ARS), Gainesville, FL 32608; [b]Section of Cell and Developmental Biology, University of California at San Diego, La Jolla, CA 92093-0380; [c]Kaplan Schiller Research, Gainesville, FL 32604; [d]Department of Environmental Systems Science, ETH Zurich, 8092 Zurich, Switzerland; [e]Cologne Biocenter/Botanical Institute, University of Cologne, 50674 Cologne, Germany; [f]Institute of Bioinformatics, University of Georgia, Athens, GA 30602; [g]Department of Genetics, University of Georgia, Athens, GA 30602; [h]Department of Plant Pathology and Microbiology, Texas A&M University, College Station, TX 77843; [i]Graduate School of Agriculture, Kyoto University, Kitashirakawa, Sakyo, 606-8502 Kyoto, Japan; [j]Boyce Thompson Institute for Plant Research, Ithaca, NY 14853; [k]Crop Genetics and Breeding Research Unit, USDA–ARS, Tifton, GA 31793; and [l]South Atlantic Area Office, USDA–ARS, Athens, GA 30605

Edited by Ian T. Baldwin, Max Planck Institute for Chemical Ecology, Jena, Germany, and approved July 27, 2015 (received for review June 9, 2015)

Plant damage promotes the interaction of lipoxygenases (LOXs) with fatty acids yielding 9-hydroperoxides, 13-hydroperoxides, and complex arrays of oxylipins. The action of 13-LOX on linolenic acid enables production of 12-oxo-phytodienoic acid (12-OPDA) and its downstream products, termed "jasmonates." As signals, jasmonates have related yet distinct roles in the regulation of plant resistance against insect and pathogen attack. A similar pathway involving 9-LOX activity on linolenic and linoleic acid leads to the 12-OPDA positional isomer, 10-oxo-11-phytodienoic acid (10-OPDA) and 10-oxo-11-phytoenoic acid (10-OPEA), respectively; however, physiological roles for 9-LOX cyclopentenones have remained unclear. In developing maize (*Zea mays*) leaves, southern leaf blight (*Cochliobolus heterostrophus*) infection results in dying necrotic tissue and the localized accumulation of 10-OPEA, 10-OPDA, and a series of related 14- and 12-carbon metabolites, collectively termed "death acids." 10-OPEA accumulation becomes wound inducible within fungal-infected tissues and at physiologically relevant concentrations acts as a phytoalexin by suppressing the growth of fungi and herbivores including *Aspergillus flavus*, *Fusarium verticillioides*, and *Helicoverpa zea*. Unlike previously established maize phytoalexins, 10-OPEA and 10-OPDA display significant phytotoxicity. Both 12-OPDA and 10-OPEA promote the transcription of defense genes encoding glutathione S transferases, cytochrome P450s, and pathogenesis-related proteins. In contrast, 10-OPEA only weakly promotes the accumulation of multiple protease inhibitor transcripts. Consistent with a role in dying tissue, 10-OPEA application promotes cysteine protease activation and cell death, which is inhibited by overexpression of the cysteine protease inhibitor maize cystatin-9. Unlike jasmonates, functions for 10-OPEA and associated death acids are consistent with specialized roles in local defense reactions.

oxylipin | 9-lipoxygenase | 10-oxo-11-phytoenoic acid | maize | defense

In plants, cellular damage results in the enzymatic and nonenzymatic peroxidation of fatty acids (FAs) termed "oxylipins." Enzymatic biosynthesis can be initiated by lipase-based cleavage of linoleic acid (18:2) or α-linolenic acid (18:3) from membrane lipids and subsequent dioxygenation by lipoxygenases (LOXs) with regiospecificity at carbons 9 or 13. Specific oxylipins function as direct antimicrobial defenses and plant signaling molecules that regulate diverse processes including development, reproduction, stress acclimation, and innate immune responses against pests and pathogens (1–3).

The most studied 13-LOX 18:3-derived plant oxylipins are 12-oxo-phytodienoic acid (12-OPDA) and jasmonic acid (JA). Biosynthesis requires conversion of 13-hydroperoxides to unstable epoxides via allene oxide synthase (AOS), cyclization by allene oxide cyclase (AOC) to form 12-OPDA, reduction of the cyclopentenone ring by 12-oxo-phytodienoic acid reductase (OPR), and subsequent β-oxidation steps to produce (+)-7-iso-JA (1, 4) (Fig. 1*F*). JA is further conjugated by jasmonate resistant 1 (JAR1) to its bioactive form, JA-Ile, which mediates formation of the Coronatine Insensitive (COI1)-Jasmonate Zim domain (JAZ) family complex to promote gene expression (5, 6). Diverse roles for JA and 12-OPDA as signals include developmental processes and inducible defenses against biotic threats (1–3, 7). Genetic evidence in maize (*Zea mays*) supports a role for JA biosynthesis in the survival of biotic stress, regulation of senescence, and cell death processes mediating male sex determination (8, 9). As a precursor, 12-OPDA can trigger developmental processes and defense signaling different from JA-Ile (10–12). During physiological stress, 12-OPDA binds cyclophilin 20–3 which facilitates recruitment of a cysteine synthase complex

Significance

In plants, 12-oxo-phytodienoic acid (12-OPDA) and jasmonic acid are key 13-lipoxygenase-derived linolenate oxidation products termed jasmonates that regulate diverse processes in development and innate immunity. A less-studied metabolic pathway branch is generated by 9-lipoxygenase activity on linoleic acid, enabling the production of 10-oxo-11-phytoenoic acid (10-OPEA). In maize, fungal infection by southern leaf blight (*Cochliobolus heterostrophus*) results in the localized production of 10-OPEA, and a series of related 12- and 14-carbon cyclopente(a)nones, collectively termed "death acids" (DAs). DAs far exceed jasmonates in abundance within infected tissues, display direct phytoalexin activity against biotic agents, mediate defense gene expression, and can promote cytotoxicity resulting in cell death. Collectively DA activities are consistent with specialized local roles in plant defense.

Author contributions: S.A.C., N.M., and E.A.S. designed research; S.A.C., A.H., S.Z., and E.A.S. performed research; S.A.C., A.H., F.K., S.Z., G.D., L.J., R.J.S., M.V.K., H.T.A., G.J., X.N., and E.A.S. contributed new reagents/analytic tools; S.A.C., A.H., F.K., J.S., L.J., R.C.S., S.B., Z.A., and E.A.S. analyzed data; and S.A.C. and E.A.S. wrote the paper.

The authors declare no conflict of interest.

This article is a PNAS Direct Submission.

Data deposition: The data reported in this paper have been deposited in the Gene Expression Omnibus (GEO) database, www.ncbi.nlm.nih.gov/geo (accession nos. GSE68589 and GSE69659).

[1]To whom correspondence should be addressed. Email: eschmelz@ucsd.edu.

This article contains supporting information online at www.pnas.org/lookup/suppl/doi:10.1073/pnas.1511131112/-/DCSupplemental.

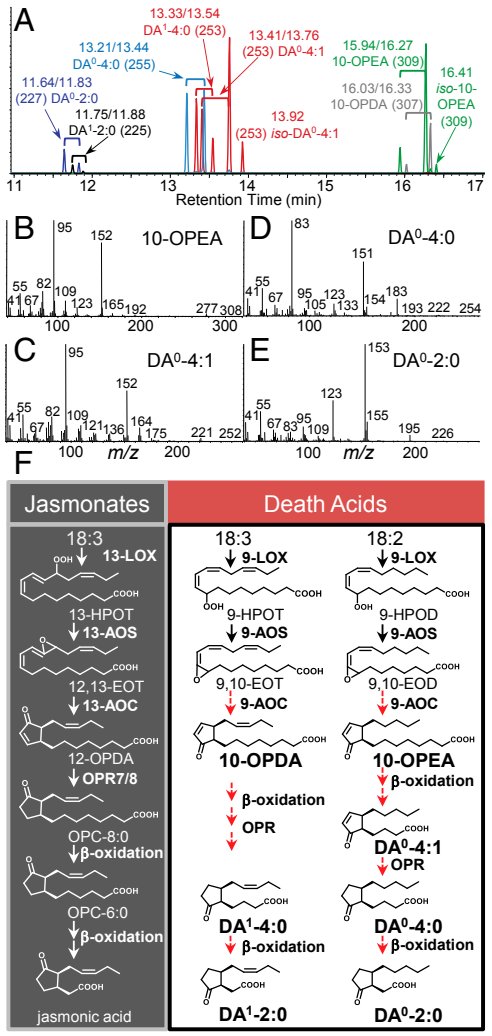

Fig. 1. Identity, spectra, and conceptual working model for the biosynthetic pathway of death acids (DAs) derived from linoleic and linolenic acid. (*A*) Combined purified standards showing GC retention times (*trans/cis* pairs: min) and predominant positive-CI MS $[M+H]^+$ ions of DA^0-2:0, DA^1-2:0, DA^0-4:0, DA^1-4:0, DA^0-4:1, iso-DA^0-4:1,10-OPEA, 10-OPDA, and iso-10-OPEA as methyl esters. Comparative EI spectra of purified linoleic acid-derived DAs as methyl esters: (*B*) 10-OPEA, (*C*) DA^0-4:1, (*D*) DA^0-4:0, and (*E*) DA^0-2:0. (*F*) Proposed model of death acid biosynthesis with respect to the jasmonic acid pathway. Red dashed arrows indicate the presence of predicted enzyme activities requiring future confirmation. Abbreviations are as follows: lipoxygenase (LOX), allene oxide synthase (AOS), allene oxide cyclase (AOC), 12-oxo-phytodienoate reductases (OPR), linolenic acid (18:3), linoleic acid (18:2), 9-hydroperoxy-10,12-octadecadienoic acid (9-HPOD), 9-hydroperoxy-10,12,15-octadecatrienoic acid (9-HPOT), 13-hydroperoxy-10,12,15-octadecatrienoic acid (13-HPOT); 9,10-epoxyoctadecatrienoic acid (9,10-EOT); 9,10-epoxyoctadecadienoic acid (9,10-EOD); 12,13-epoxyoctadecatrienoic acid (12,13-EOT); 10-oxo-11,15-phytodienoic acid (10-OPDA); 10-oxo-11-phytoenoic acid (10-OPEA); 12-oxo-10,15-phytodienoic acid (12-OPDA); 3-oxo-2-(2′-pentenyl)-cyclopentane-1-octanoic acid (OPC-8:0), and hexanoic acid (OPC-6:0).

leading to elevated glutathione levels and cellular redox homeostasis (11). 12-OPDA signaling is partly dependent upon TGA transcription factors that govern detoxification responses such as OPRs, glutathione S transferases (GSTs) and cytochrome P-450s (CYPs) consistent with a role in cell protection and survival (13, 14). The activity of structurally related nonenzymatic cyclopentenone oxylipins, such as the phytoprostanes, overlap with 12-OPDA–regulated defense responses (13, 15, 16). In the context of nonenzymatic lipid signals, many reactive electrophile species can promote cell protection by inducing genes responsible for detoxification, cell cycle regulation, and chaperones (17).

In addition to jasmonates, specific 9-LOX oxylipins also influence seed germination, root growth, and senescence as well as mediation of either susceptibility or resistance to pests and pathogens (18–22). As direct defenses, 9-LOX oxylipins can act as phytoalexins; for example, colneleic and colnelenic acids are pathogen inducible and inhibitory to *Phytophthora infestans* (23). As mediators, metabolites derived from the 9-LOX pathway in pepper (*Capsicum annuum*) and *Arabidopsis* positively regulate defense and cell death responses to diverse pathogens (21). Despite numerous studies linking the 9-LOX pathway to cell death processes (24–26), many oxylipin identities, activities, and links to enzyme activation remain unknown (27, 28). As a positional isomer of 12-OPDA, the 9-LOX oxylipin 10-oxo-11,15-phytodienoic acid (10-OPDA) and the 18:2-derived 10-oxo-11-phytoenoic acid (10-OPEA) are structurally similar to jasmonates (29). In potato (*Solanum tuberosum*), *cis*-10-OPEA is formed as a racemic product of 9-AOS–derived 9,10-epoxyoctadecadienoic acid (9,10-EOD) that is inefficiently cyclized in the absence of AOC (29, 30). Similarly, the 9-LOX/AOS pathway in tomato (*Solanum lycopersicum*) can act on 18:3 to yield 10-OPDA (31). These studies draw attention to the possibility of downstream 9-LOX derivatives of 10-OPEA and 10-OPDA; however, the existence of additional jasmonate-like metabolites has remained elusive.

While searching for defense-related metabolites present in southern leaf blight (SLB; *Cochliobolus heterostrophus*) infected maize, we detected high levels of 10-OPEA and a series of related cyclopente(a)none oxylipins. Localized within dying and necrotic tissues, we collectively refer to 10-OPEA, 10-OPDA, and derivatives as "death acids" (DAs). As direct defenses, levels of 10-OPEA produced in diseased tissues after wounding match those of known maize phytoalexins [>100 $\mu g \cdot g^{-1}$ fresh weight (FW)] and can impair growth in pathogens, insects, and plant cells. In contrast to 10-OPEA and 10-OPDA, previously established maize phytoalexins sharing reactive α,β-unsaturated carbonyls lack significant phytotoxicity in maize. Exogenous application of 10-OPEA to plant tissues strongly induces defense genes, cysteine protease activity, and common cell death symptoms including lesions, ion leakage, and DNA fragmentation. Unlike JA and 12-OPDA, 10-OPEA and related DAs elicit significantly lower transcriptional up-regulation of multiple protease inhibitors (PIs) including the maize cystatin-9 (*ZmCC9*), a negative regulator of apoplastic mediated cell death (27). Overexpression of *ZmCC9* reduces the extent of 10-OPEA–induced lesions and provides a mechanistic link to the cytotoxic action in maize.

Results and Discussion

Identity of Cyclopente(a)none Death Acids in Maize. To elucidate pathogen-induced defense metabolites in maize, we conducted metabolic profiling of SLB-infected tissues. Among the analytes were the rarely encountered 9-LOX derived cyclopentenones, 10-OPEA, 10-OPDA, and seven other related yet unknown cyclopente(a)nones (Fig. 1*A*) (29, 31). To establish identities, we performed a large-scale purification of these analytes and used ^1H and ^{13}C NMR spectroscopy (*SI Appendix*, Table S1). Chemical and electron ionization (CI/EI) mass spectrometry of the corresponding methyl esters provides useful diagnostic spectra of these 10-OPEA and 10-OPDA derivatives (Fig. 1 *B–E* and *SI Appendix*, Fig. S1). Additional related isomerization products of 10-OPEA, including *iso*-10-OPEA were also identified (*SI Appendix*, Table S1) (29). Given multiple FA precursors and additional anticipated metabolites, we assigned each DA according to the number of carbons in the carboxylic acid side chain (e.g., DA-X), the presence/absence of a double bond in the cyclopente (a)none ring (e.g., DA-X:1 or DA-X:0), and its FA origin (e.g., 18:2 = DA^0; 18:3 = DA^1). In our proposed model, DA biosynthesis

initiates with 9-LOX activity on 18:2 and 18:3 to form 9-hydroperoxides followed by 9-AOS–mediated allene oxide formation (30, 31). Analysis of *ZmLOX* and *ZmAOS* gene expression from SLB-infected leaves indicated that *ZmLOX3/4/5* and *ZmAOS1/3* are candidate genes for the initial steps in pathogen-induced DA biosynthesis (*SI Appendix*, Fig. S2). SLB-infection screening of available single and double LOX mutants, including *Zmlox3*, *Zmlox4*, *Zmlox5*, *Zmlox3/5*, and *Zmlox4/5*, showed no significant reduction in 10-OPEA production (*SI Appendix*, Fig. S2). This suggests that multiple LOXs provide substrates for DA biosynthesis, similar to the complexity observed for JA biosynthesis (32). In contrast to the AOC-mediated enzymatic cyclization of 12,13-epoxyoctadecatrienoic acid yielding pure (9*S*,13*S*)-12-OPDA [i.e., *cis*(+)-12-OPDA] in potato and tomato, *cis*-10-OPEA and *cis*-10-OPDA are formed as minor racemic (9*S*,13*S* and 9*R*,13*R*) cyclization products of AOS-derived 9-allene oxides, which are predominantly hydrolyzed to α-ketols (29, 30, 33). Analysis of these relationships in maize unexpectedly revealed that inducible levels of *cis*-10-OPEA exceeded those of the predicted dominant α-ketol (9-hydroxy-10-oxo-12(*Z*)-octadecenoic acid) product by more than 15-fold (*SI Appendix*, Fig. S3). Chiral phase high performance liquid chromatography (CP-HPLC) analysis of maize *cis*-10-OPEA was then performed and resulted in a single chromatographic peak, whereas a standard of racemic (9*S*,13*S* and 9*R*,13*R*) *cis*-10-OPEA produced two separate peaks (*SI Appendix*, Fig. S3). Our results are consistent with recently published findings demonstrating that maize synthesis of predominantly (9*S*,*13S*)-10-OPEA is enzymatic and is the result of an undiscovered AOC acting on 9-LOX derived allene oxide(s) (34). Curiously, a portion of the 10-OPEA cyclopentenone appears to undergo two β-oxidation–like steps to form DA^0-4:1 before an OPR-like mediated cyclopentenone reduction to DA^0-4:0 (Fig. 1*F* and *SI Appendix*, Fig. S4). This differs from the JA biosynthetic pathway where OPR activity first reduces *cis*-12-OPDA to a cyclopentanone. Additional processing of DA^0-4:0 and DA^1-4:0 by a β-oxidation step is envisioned to produce the 9-LOX positional isomers of dihydro-JA and JA, respectively denoted as DA^0-2:0 and DA^1-2:0. To investigate the capacity of healthy control maize plants to synthesize processed DA pathway metabolites, we applied *cis*-10-OPEA to leaves and observed the accumulation of C14 and C12 DAs within 2 h (*SI Appendix*, Fig. S4). Although not excluding the potential for multiple origins in nature, these results establish the capacity of maize to produce cyclopente(a)none DAs.

10-OPEA Acts as a Cytotoxic Phytoalexin. To compare the dynamics of DA accumulation to structurally related oxylipins and defense signals, both SLB-infected (local) and adjacent tissues (distal, 1–2 mm from the site of visible necrosis) were analyzed over 48 h. Within 24 h, local infected tissues displayed 8-fold increases in salicylic acid (SA) and 10-OPEA accumulation, whereas 12-OPDA and JA concentrations only moderately increased (Fig. 2 *A*–*C* and *H*). By 48 h, 10-OPEA concentrations within local infected tissues predominated over SA, JA, and 12-OPDA by >5-fold. Accumulation of DA^0-4:0 and DA^0-2:0 also significantly increased by 48 h, suggesting active processing of 10-OPEA in plants during disease progression (Fig. 2 *G* and *I*). Interestingly, the 18:3 derivatives 10-OPDA and DA^1-4:0 were 7- and 2-fold lower than 10-OPEA and DA^0-4:0 in SLB-infected tissues, respectively, consistent with a tissue bias in 18:2 precursor present (*SI Appendix*, Fig. S5). In the tissue distal to SLB infection, SA accumulation was 6-fold higher than mechanically damaged controls (Fig. 2*D*); however, there was little or no distal accumulation of 12-OPDA or 10-OPEA family DAs at 48 h (Fig. 2 E and *J*–*L*). Thus, DA production is localized and confined to diseased tissue. In an attempt to mimic the collapse of plant cells under pathogen attack, tissues were subsequently crush damaged either 2 or 4 d after SLB inoculation. Damaged plants with subsequent crush damage produced high levels of 18:2 and 18:3, yet 10-OPEA, 10-OPDA, DA^0-4:0, DA^1-4:0, and DA^0-2:0

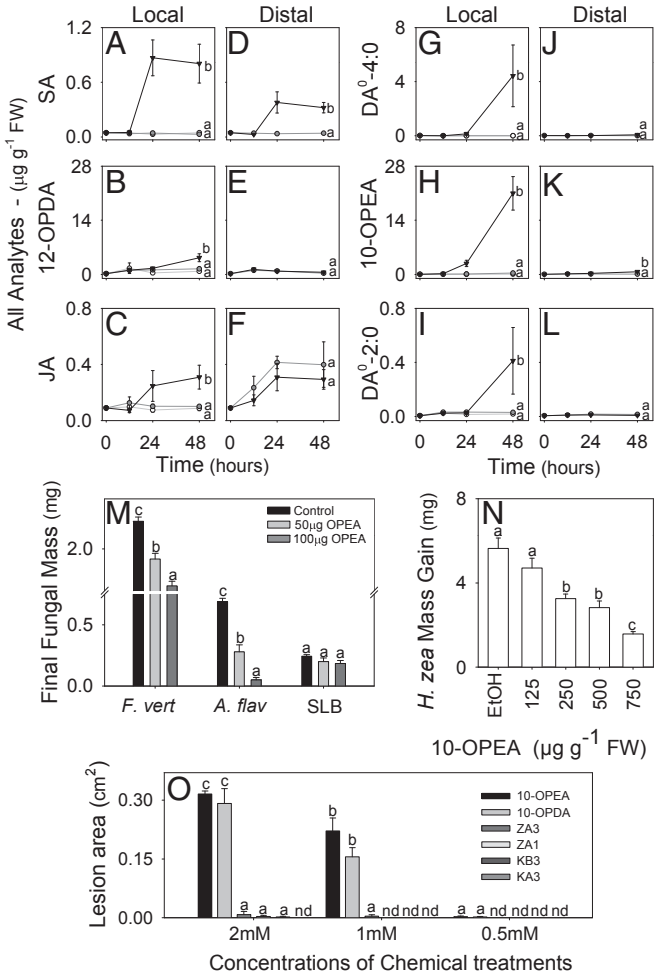

Fig. 2. DAs predominate in localized diseased tissue and display antimicrobial, antiinsect, and phytotoxic activity. Average ($n = 4$, ± SEM) concentrations (μg·g^{-1} FW) of (*A* and *D*) SA, (*B* and *E*) 12-OPDA, (*C* and *F*) JA, (*G* and *J*) DA^0-4:0, (*H* and *K*) 10-OPEA, and (*I* and *L*) DA^0-2:0 in maize interior whorl tissue following no treatment (open circle), mechanical incision damage (gray circle), and SLB inoculation (solid triangle). Two segments consisting of the infected site (local; *A*–*C* and *G*–*I*) and visually asymptomatic tissue 1–2 mm adjacent to the treatment site (distal; D–*F* and *J*–*L*) were collected for analysis at indicated times. (*M*) Average ($n = 8$, ± SEM) southern leaf blight (SLB), *Fusarium verticillioides (F.v.)*, and *Aspergillus flavus (A.f.)* hyphae mass (in milligrams) after 72 h in media containing 0, 50, or 100 μg·ml^{-1} 10-OPEA. (*N*) Average mass gain (in milligrams) ($n = 20$, ± SEM) in *H. zea* larval growth after 24 h on maize leaf diet containing 10-OPEA (125–750 μg·g^{-1} FW). (*O*) Average ($n = 4$, ± SEM) maize leaf lesion area (in square centimeters) at 24 h for phytoalexin toxicity analysis. Fourth leaves were treated with two 10-μL droplets of 10-OPEA, 10-OPDA, zealexins (Z; ZA1 and ZA3) and kauralexins (K; KA3 and KB3) at concentrations of 0.5, 1, and 2 mM dissolved in 95:5:0.1 H_2O:DMSO:Tween 20 (vol/vol/vol). Within plots, different letters (*a*–*d*) represent significant differences at indicated time points (nd, not detected; all ANOVA $P < 0.05$; Tukey test for corrections for multiple comparisons: $P < 0.05$).

levels remained very low (Fig. 2 and *SI Appendix*, Figs. S5 and S6). In contrast, SLB-infected tissue subjected to subsequent crush damage resulted in 10-OPEA accumulation exceeding 150 μg·g^{-1} FW, which surpassed 12-OPDA and JA production by >7-fold (*SI Appendix*, Figs. S5 and S6). On average, diseased tissues also produced higher levels of DA^0-4:0 and DA^0-2:0 in response to crush damage, surpassing JA levels by 15- and 3-fold, respectively.

Collectively, wound-induced accumulation of 10-OPDA and 10-OPEA in SLB-infected tissues and damaged silks can range between 180 and 340 μg·g^{-1} FW (*SI Appendix*, Figs. S5–S7)

concentrations similar to fungal induced levels of terpenoid phytoalexins (35, 36). Given that oxylipins can function as phytoalexins, we investigated the potential for 10-OPEA to act as a direct defense (23, 37). 10-OPEA displayed minor inhibitory effects against SLB growth in vitro, suggesting appreciable fungal tolerance or detoxification (Fig. 2*M*). Conversely, growth of *Fusarium verticillioides* and *Aspergillus flavus* was significantly suppressed by 10-OPEA at 100 $\mu g \cdot mL^{-1}$ (Fig. 2*M*) and is consistent with the variation in fungal species tolerance observed in oxylipin antimicrobial assays (38). Given the abundance of 10-OPEA wounded silks and modest accumulation in stems following 6 d of corn earworm (CEW; *Helicoverpa zea*) herbivory (*SI Appendix*, Fig. S7), we examined a role for 10-OPEA as an insect growth inhibitor. Over a range of 125–750 $\mu g \cdot g^{-1}$ FW, 10-OPEA promoted a concentration-dependent inhibition of insect growth (Fig. 2*N*). These results indicate that 10-OPEA can function as a broadly active phytoalexin that shares similar antibiotic potencies to maize zealexins and kauralexins (35, 36). Because phytoalexins can also harm plant cells (39), we tested the cytotoxic properties of 10-OPEA in comparison with four different maize phytoalexins (zealexin A1/A3, kauralexin A3/B3). Comparatively, 10-OPEA and 10-OPDA were equally cytotoxic and resulted in 35-fold greater lesion areas than acidic terpenoid phytoalexins tested (Fig. 2*O*).

10-OPEA and DA^0-4:0 Mediate Defense Gene Expression. Given that cyclopentenones and cyclopentanones can have distinct signaling properties, we first investigated the potential for 10-OPEA–mediated transcriptional regulation using the Affymetrix GeneChip maize genome array (7, 12, 16). Treatment with 10-OPEA after 90 min resulted in 55 genes with a twofold or greater change in probe intensity at 95% confidence. Among the strongest induced transcripts were genes associated with OPR activity, pathogen defense, cell death, calcium signaling, and redox homeostasis (*SI Appendix*, Dataset S1). To validate the microarray results and to compare 10-OPEA activity to other meaningful metabolites, we treated plants with either SA, 12-OPDA, JA, 10-OPEA, DA^0-4:0, or SLB and compared the expression levels of pathogen- and insect-related genes at 3 h using qRT-PCR. Defense marker genes included *ZmOPR2*, the maize OPR most strongly up-regulated in response to SLB (40); pathogenesis-related 4b (*ZmPR4b*) and EF-hand Ca^{2+}-binding protein (*ZmCCD1*), genes involved in the promotion of cell death and pathogen-elicited defense responses (41–43); GST 2 (*ZmGST2*) and hydrolase (*ZmHYD*), previously shown to be induced by both insect- and pathogen-related treatments (35, 44); a stress-inducible oxidoreductase (*ZmOXR*); and maize cystatin 9 (*ZmCC9*), wound inducible protein 1 (*ZmWIP1*), and serine protease inhibitor (*ZmSerPIN*), that encode PIs inducible by biotic attack (27, 45, 46). The defense genes *ZmPR4b*, *ZmOPR2*, and *ZmCCD1* were strongly induced by 10-OPEA and DA^0-4:0 treatments with expression levels either statistically equivalent to or higher than those of 12-OPDA, JA, and SA (Fig. 3 *A*–*C*). The insect- and pathogen-inducible transcripts encoding *ZmGST2* and *ZmHYD* were also significantly up-regulated by 10-OPEA and DA^0-4:0 (Fig. 3 *D* and *E*), suggesting functional overlap with maize responses to biotic stress. Curiously, *ZmOXR* transcript accumulation was more responsive to SA than all other treatments (Fig. 3*F*). Whereas similar expression patterns between DAs and established signals were observed in other defense genes (*SI Appendix*, Fig. S8), there was a consistent difference between DAs and jasmonates in the expression of multiple PIs. As expected, transcript accumulation of pathogen- and insect-inducible PIs was strongly regulated by JA and 12-OPDA; however, 10-OPEA and DA^0-4:0 resulted in significantly lower PI transcript accumulation (Fig. 3 *G*–*I*). Compared with jasmonates, weak DA-mediated PI transcriptional regulation may leave respective protease activities unaltered. To identify additional responses, we subsequently performed whole transcriptome

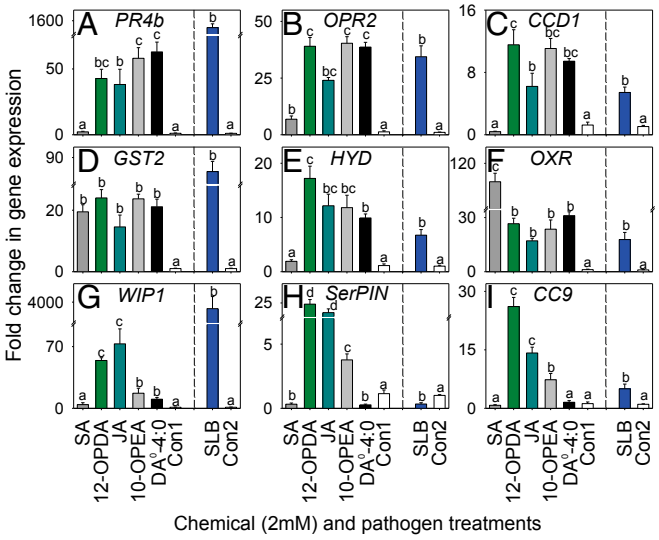

Fig. 3. 10-OPEA and DA^0-4:0 induce defense gene expression in maize. Average (n = 4, ± SEM) qRT-PCR fold change in transcript levels of genes encoding pathogen and insect defense proteins including (*A*) *ZmPR4b*, (*B*) *ZmOPR2*, (*C*) *ZmCCD1*, (*D*) *ZmGST2*, (*E*) *ZmHYD*, (*F*) *ZmOXR*, (*G*) *ZmWIP1*, (*H*) *ZmSerPIN*, and (*I*) *ZmCC9*, 3 h posttreatment (all 2 mM) with SA (dark gray), 12-OPDA (light green), JA (dark green), 10-OPEA (light gray), DA^0-4:0 (black), or control (white; Con1: 95:5:0.1 H_20:DMSO:Tween 20, vol/vol/v), or 24 h postinfection with SLB spores (blue bar) and H_20 with 0.1% Tween 20 (white; Con2). Within chemical- and SLB-infection treatment plots, different letters (*a*–*d*) represent significant differences (all ANOVA $P < 0.05$; Tukey test corrections for multiple comparisons: $P < 0.05$).

analyses using RNA-Seq. In this experiment, 10-OPEA and 12-OPDA treatments resulted in over 5,000 differentially expressed candidate genes with 60% being either equally elicited or suppressed by both cyclopentenones at 3 h (*SI Appendix*, Dataset S2). Enrichment analyses of transcripts displaying comparatively stronger elicitation to 10-OPEA than 12-OPDA were dominated by heat shock proteins (HSPs) and GSTs (*SI Appendix*, Table S2). Transcript accumulation specific to 10-OPEA treatments encodes proteins that function in transport and detoxification (e.g., P450s). Conversely, enrichment of transcripts displaying comparatively stronger elicitation to 12-OPDA than 10-OPEA were dominated by genes associated with aromatic amino acid biosynthesis, secondary metabolism, and jasmonate regulation. Importantly, 12-OPDA application results in partial conversion to JA and thus the combination of two distinct jasmonate pathway responses (12, 13). Compared with 10-OPEA, 12-OPDA specific transcripts are enriched for encoded proteins predicted to function in cell wall synthesis. Collectively, these analyses confirm a broad coregulation of the 12-OPDA and 10-OPEA transcriptome (Fig. 3) with narrow subsets of gene ontology enrichments consistent with defense and cell fortification for 12-OPDA and detoxification, molecular chaperones (HSPs), and transport for 10-OPEA (*SI Appendix*, Dataset S2 and Table S2).

10-OPEA Cytotoxicity Is Mediated by a Cysteine Protease Inhibitor. Given DA accumulation in necrotic tissue, comparatively high cytotoxicity, and weak induction of both *ZmCC9* and *ZmSerPIN*, established inhibitors of cysteine protease-mediated cell death (27, 45), we hypothesized that high concentrations of 10-OPEA may function as a positive mediator of cell death. To compare lesion-inducing activity, we examined leaves treated with 10-OPEA, DA^0-4:0, DA^0-4:1, *iso*-10-OPEA, 18:2, 18:3, and the phytohormones JA, 12-OPDA, and SA (1, 47). Fumonisin B1 (FB1), a cell death inducing mycotoxin, was also included (48). Little or no visual evidence for cell death was found in either SA,

JA, FB1, or solvent control treated plants at 24 h (Fig. 4*A*). However, significant cell death was observed in 10-OPEA–treated leaves with chlorotic lesion areas at least twofold larger than all other treatments (Fig. 4*A*). Interestingly, DA^0-4:1 contains an α,β-unsaturated carbonyl similar to 10-OPEA and 12-OPDA yet lesion promotion was greatly reduced. This suggests that the presence of a Michael addition site alone does not control the observed toxicity (17). Similarly, within 5 h, electrolyte leakage in 10-OPEA–treated leaves was at least twofold greater than all other treatments and remained significantly higher over a 15-h period (Fig. 4*B* and *SI Appendix*, Fig. S9). DNA fragmentation was also observed in tissues treated with 1–4 mM 10-OPEA, a response consistent with cell death (Fig. 4*A*)

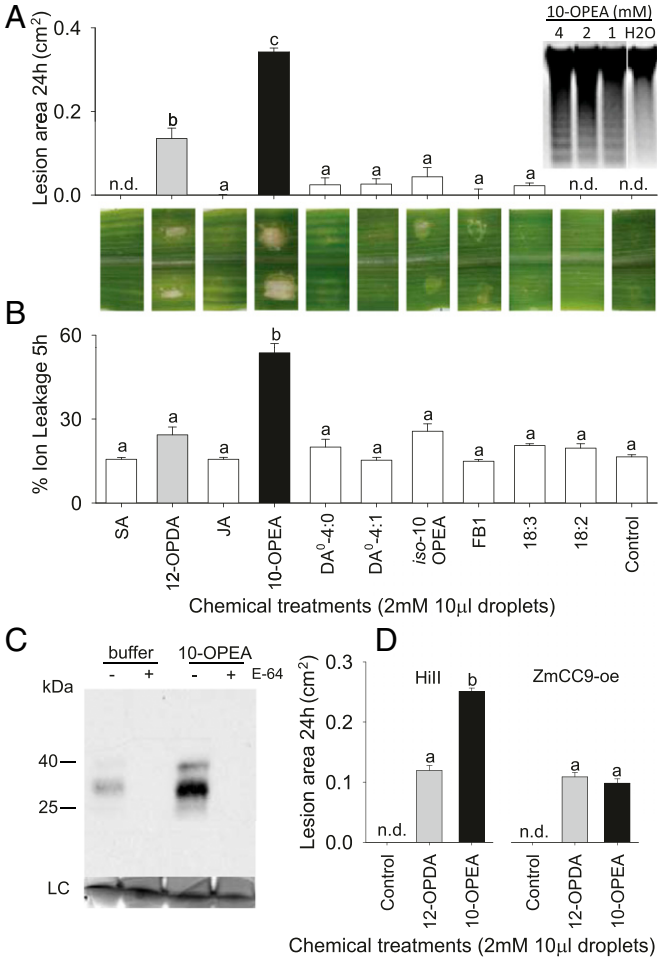

Fig. 4. 10-OPEA promotes lesions in maize. (*A*) Quantification (in square centimeters) of macroscopic lesions (cell death) at 24 h and (*B*) leaf disk percent (%) ion leakage at 5 h following treatment with two droplets (all 2 mM) of SA, 12-OPDA (gray), JA, 10-OPEA (black), DA^0-4:0, DA^0-4:1, *iso*-10-OPEA, fumonisin B1 (FB1), 18:3 (linolenic acid), 18:2 (linoleic acid), or control solution (95:5:0.1 H_20:DMSO:Tween 20, vol/vol/v). Reflective surface deposits were examined and excluded if lacking lesions. (*A*, *Insert*) DNA fragmentation from leaf midrib tissue 4 h following treatment with 4, 2, and 1 mM 10-OPEA and H_2O control. (*C*) Activity-based protein profiling demonstrates activation of cysteine proteases by 10-OPEA. Immunoblot detection of DCG-04–labeled leaf extracts 8 h posttreatment with 2 mM 10-OPEA. Extracts were pretreated with 5 μM E-64, or untreated, and thereafter labeled with DCG-04. (*D*) Inhibition of papain-like cysteine proteases significantly reduces 10-OPEA–mediated cell death at 24 h. Wild type (HiII) and ZmCC9-overexpression (oe) plants were treated with two 10-μL droplets of 2 mM 10-OPEA, 12-OPDA, or control solution. Within plots, different letters (*a*–*c*) represent significant differences (all ANOVA $P < 0.05$; Tukey test corrections for multiple comparisons: $P < 0.05$; nd, not detected).

(49, 50). As cell death processes are often mediated by cysteine proteases (27, 28), we examined the capacity of 10-OPEA to induce cysteine protease activity using DCG-04, a biotinylated substrate that reacts with the catalytic cysteine residue of papain-like cysteine proteases. Immunoblot detection of DCG-04–labeled proteases from leaf tissue collected 8 h posttreatment with 10-OPEA showed stable induction of protease activity, indicated by two bands with the expected masses of 30 and 40 kDa (Fig. 4*C*). Preincubation with the cysteine protease inhibitor E-64 blocked protease labeling, confirming specificity of the probe. To genetically test if inhibition of cysteine protease activity impairs 10-OPEA–induced lesions, wild-type (HiII) plants and those overexpressing (oe) the papain-like cysteine PI ZmCC9 (ZmCC9-oe) (27) were comparatively treated with 10-OPEA and 12-OPDA (Fig. 4*D*). At 24 h, 10-OPEA–induced lesion areas were twofold greater than 12-OPDA as expected (Fig. 4 *A* and *D*); however, on ZmCC9-oe plants there was no significant difference between 10-OPEA and 12-OPDA. Collectively, these results are consistent with 10-OPEA acting as a broadly toxic phytoalexin with the additional capacity to activate cysteine proteases and promote cell death, which is negatively regulated in part by ZmCC9. As pathogenic fungi are known to manipulate host lipid metabolism to facilitate pathogenicity (51), we used wild-type HiII and ZmCC9oe plants to investigate whether SLB uses 10-OPEA to promote necrotrophy via cysteine protease-mediated cell death. Three days post-SLB inoculation, ZmCC9oe plants showed no difference in lesion areas compared with HiII (*SI Appendix*, Fig. S10). Curiously, interior whorl SLB infection on HiII and ZmCC9oe plants revealed higher 10-OPEA levels in ZmCC9oe plants than HiII (*SI Appendix*, Fig. S10). Although speculative, these results hint at the existence of localized homeostatic compensation in 10-OPEA production to counter ZmCC9oe-mediated cell death inhibition ultimately returning the phenotype to wild-type HiII lesion levels. Alternatively, the lack of lesion area differences between SLB-infected HiII and ZmCC9oe plants suggests that SLB does not rely upon 10-OPEA cytotoxicity and cysteine protease-activated cell death for pathogenicity.

The existence of a 9-LOX initiated pathway conceptually similar to the 13-LOX jasmonate pathway was postulated 15 y ago when 10-OPEA and 10-OPDA production was first observed in potato homogenates (29). Our investigation of pathogen-elicited maize oxylipins enabled the discovery of 9-LOX–derived cyclopente(a)none DAs and the characterization of 10-OPEA as a directly defensive phytoalexin with significant cytotoxicity. 10-OPEA is also the source of nontoxic cyclopente(a)nones both of which have transcriptional activity. The most critical immediate question left unanswered is "do maize plants lacking 10-OPEA biosynthesis display altered biotic or abiotic stress responses?" Given the current work and recently published findings, the most elegant way to address this issue will be the identification of the AOC(s) responsible for 10-OPEA biosynthesis and creation of null mutant plants (34). Additional remaining questions involve the occurrence and function of DAs in multiple grain crops, the role of individual DAs as transcriptional mediators, and mechanistic basis for differential activity in gene expression. Although not as commonly encountered as jasmonates, in maize, DAs have selective localized activities consistent with defense and stress response mediation.

Materials and Methods

The isolation and identification of acidic maize metabolites follows from Schmelz et al. (36) with modification (*SI Appendix, SI Materials and Methods*). Quantification of maize metabolites by gas chromatography-mass spectrometry, chemical treatment of plants and bioassays with *C. heterostrophus*, *A. flavus*, and *F. verticillioides* follows from Huffaker et al. (35) as detailed (*SI Appendix, SI Materials and Methods*). Unless otherwise noted, all experiments in this work consisted of at least four or more independent biological replicates. Additional details on experimental protocols and methods on can be found in *SI Appendix*.

ACKNOWLEDGMENTS. Special thanks to Wayne Davis for the kind donation of maize tissues and James R. Rocca for facilitating NMR experiments at the McKnight Brain Institute (National High Magnetic Field Laboratory, Advanced Magnetic Resonance Imaging and Spectroscopy Facility). NMR work was supported by the National Science Foundation (NSF) Division of Materials Research Award 1157490, the State of Florida, and NIH Award S10RR031637. Research was funded by US Department of Agriculture (USDA)–Agricultural Research Service Projects 6615-21000-010-00/-22000-027-00, NSF Division of Integrative Organismal Systems Competitive Award 1139329, and University of California, San Diego startup funds allocated to E.A.S.

1. Wasternack C, Hause B (2013) Jasmonates: Biosynthesis, perception, signal transduction and action in plant stress response, growth and development. An update to the 2007 review in Annals of Botany. *Ann Bot (Lond)* 111(6):1021–1058.
2. Farmer EE, Alméras E, Krishnamurthy V (2003) Jasmonates and related oxylipins in plant responses to pathogenesis and herbivory. *Curr Opin Plant Biol* 6(4):372–378.
3. Howe GA, Jander G (2008) Plant immunity to insect herbivores. *Annu Rev Plant Biol* 59:41–66.
4. Koo AJK, Chung HS, Kobayashi Y, Howe GA (2006) Identification of a peroxisomal acyl-activating enzyme involved in the biosynthesis of jasmonic acid in Arabidopsis. *J Biol Chem* 281(44):33511–33520.
5. Katsir L, Chung HS, Koo AJK, Howe GA (2008) Jasmonate signaling: A conserved mechanism of hormone sensing. *Curr Opin Plant Biol* 11(4):428–435.
6. Sheard LB, et al. (2010) Jasmonate perception by inositol-phosphate-potentiated COI1-JAZ co-receptor. *Nature* 468(7322):400–405.
7. Dave A, Graham IA (2012) Oxylipin signaling: A distinct role for the jasmonic acid precursor *cis*-(+)-12-oxo-phytodienoic acid (*cis*-OPDA). *Front Plant Sci* 3:42.
8. Acosta IF, et al. (2009) tasselseed1 is a lipoxygenase affecting jasmonic acid signaling in sex determination of maize. *Science* 323(5911):262–265.
9. Yan Y, et al. (2012) Disruption of OPR7 and OPR8 reveals the versatile functions of jasmonic acid in maize development and defense. *Plant Cell* 24(4):1420–1436.
10. Böttcher C, Pollmann S (2009) Plant oxylipins: Plant responses to 12-oxo-phytodienoic acid are governed by its specific structural and functional properties. *FEBS J* 276(17):4693–4704.
11. Park S-W, et al. (2013) Cyclophilin 20-3 relays a 12-oxo-phytodienoic acid signal during stress responsive regulation of cellular redox homeostasis. *Proc Natl Acad Sci USA* 110(23):9559–9564.
12. Stintzi A, Weber H, Reymond P, Browse J, Farmer EE (2001) Plant defense in the absence of jasmonic acid: The role of cyclopentenones. *Proc Natl Acad Sci USA* 98(22):12837–12842.
13. Mueller S, et al. (2008) General detoxification and stress responses are mediated by oxidized lipids through TGA transcription factors in Arabidopsis. *Plant Cell* 20(3):768–785.
14. Danon A, Miersch O, Felix G, Camp RG, Apel K (2005) Concurrent activation of cell death-regulating signaling pathways by singlet oxygen in *Arabidopsis thaliana*. *Plant J* 41(1):68–80.
15. Thoma I, et al. (2003) Cyclopentenone isoprostanes induced by reactive oxygen species trigger defense gene activation and phytoalexin accumulation in plants. *Plant J* 34(3):363–375.
16. Mueller MJ (2004) Archetype signals in plants: The phytoprostanes. *Curr Opin Plant Biol* 7(4):441–448.
17. Farmer EE, Mueller MJ (2013) ROS-mediated lipid peroxidation and RES-activated signaling. *Annu Rev Plant Biol* 64:429–450.
18. Vellosillo T, et al. (2007) Oxylipins produced by the 9-lipoxygenase pathway in Arabidopsis regulate lateral root development and defense responses through a specific signaling cascade. *Plant Cell* 19(3):831–846.
19. Nalam VJ, Keeretaweep J, Sarowar S, Shah J (2012) Root-derived oxylipins promote green peach aphid performance on Arabidopsis foliage. *Plant Cell* 24(4):1643–1653.
20. López MA, et al. (2011) Antagonistic role of 9-lipoxygenase-derived oxylipins and ethylene in the control of oxidative stress, lipid peroxidation and plant defence. *Plant J* 67(3):447–458.
21. Hwang IS, Hwang BK (2010) The pepper 9-lipoxygenase gene CaLOX1 functions in defense and cell death responses to microbial pathogens. *Plant Physiol* 152(2):948–967.
22. Gao X, et al. (2007) Disruption of a maize 9-lipoxygenase results in increased resistance to fungal pathogens and reduced levels of contamination with mycotoxin fumonisin. *Mol Plant Microbe Interact* 20(8):922–933.
23. Weber H, Chételat A, Caldelari D, Farmer EE (1999) Divinyl ether fatty acid synthesis in late blight-diseased potato leaves. *Plant Cell* 11(3):485–494.
24. Sun L, et al. (2014) Cotton cytochrome P450 CYP82D regulates systemic cell death by modulating the octadecanoid pathway. *Nat Commun* 5:5372.
25. Rustérucci C, et al. (1999) Involvement of lipoxygenase-dependent production of fatty acid hydroperoxides in the development of the hypersensitive cell death induced by cryptogein on tobacco leaves. *J Biol Chem* 274(51):36446–36455.
26. Montillet JL, et al. (2005) Fatty acid hydroperoxides and H_2O_2 in the execution of hypersensitive cell death in tobacco leaves. *Plant Physiol* 138(3):1516–1526.
27. van der Linde K, et al. (2012) A maize cystatin suppresses host immunity by inhibiting apoplastic cysteine proteases. *Plant Cell* 24(3):1285–1300.
28. Solomon M, Belenghi B, Delledonne M, Menachem E, Levine A (1999) The involvement of cysteine proteases and protease inhibitor genes in the regulation of programmed cell death in plants. *Plant Cell* 11(3):431–444.
29. Hamberg M (2000) New cyclopentenone fatty acids formed from linoleic and linolenic acids in potato. *Lipids* 35(4):353–363.
30. Grechkin AN, et al. (2008) Tomato CYP74C3 is a multifunctional enzyme not only synthesizing allene oxide but also catalyzing its hydrolysis and cyclization. *ChemBioChem* 9(15):2498–2505.
31. Itoh A, Schilmiller AL, McCaig BC, Howe GA (2002) Identification of a jasmonate-regulated allene oxide synthase that metabolizes 9-hydroperoxides of linoleic and linolenic acids. *J Biol Chem* 277(48):46051–46058.
32. Chauvin A, Caldelari D, Wolfender J-L, Farmer EE (2013) Four 13-lipoxygenases contribute to rapid jasmonate synthesis in wounded *Arabidopsis thaliana* leaves: A role for lipoxygenase 6 in responses to long-distance wound signals. *New Phytol* 197(2):566–575.
33. Laudert D, et al. (1997) Analysis of 12-oxo-phytodienoic acid enantiomers in biological samples by capillary gas chromatography-mass spectrometry using cyclodextrin stationary phases. *Anal Biochem* 246(2):211–217.
34. Ogorodnikova AV, et al. (2015) Stereospecific biosynthesis of (*9S,13S*)-10-oxo-phytoenoic acid in young maize roots. *Biochim Biophys Acta* 1851(9):1262–1270.
35. Huffaker A, et al. (2011) Novel acidic sesquiterpenoids constitute a dominant class of pathogen-induced phytoalexins in maize. *Plant Physiol* 156(4):2082–2097.
36. Schmelz EA, et al. (2011) Identity, regulation, and activity of inducible diterpenoid phytoalexins in maize. *Proc Natl Acad Sci USA* 108(13):5455–5460.
37. Shimada TL, et al. (2014) Leaf oil body functions as a subcellular factory for the production of a phytoalexin in Arabidopsis. *Plant Physiol* 164(1):105–118.
38. Prost I, et al. (2005) Evaluation of the antimicrobial activities of plant oxylipins supports their involvement in defense against pathogens. *Plant Physiol* 139(4):1902–1913.
39. Bhandal IS, Paxton JD, Widholm JM (1987) *Phytophthora megasperma* culture filtrate and cell-wall preparation stimulate glyceollin production and reduce cell viability in suspension-cultures of soybean. *Phytochemistry* 26(10):2691–2694.
40. Zhang J, et al. (2005) Genomic analysis of the 12-oxo-phytodienoic acid reductase gene family of *Zea mays*. *Plant Mol Biol* 59(2):323–343.
41. Hemetsberger C, Herrberger C, Zechmann B, Hillmer M, Doehlemann G (2012) The *Ustilago maydis* effector Pep1 suppresses plant immunity by inhibition of host peroxidase activity. *PLoS Pathog* 8(5):e1002684.
42. Hwang IS, Choi S, Kim NH, Kim DS, Hwang BK (2014) Pathogenesis-related protein 4b interacts with leucine-rich repeat protein 1 to suppress PR4b-triggered cell death and defense response in pepper. *Plant J* 77(4):521–533.
43. Takezawa D (2000) A rapid induction by elicitors of the mRNA encoding CCD-1, a 14 kDa Ca^{2+} -binding protein in wheat cultured cells. *Plant Mol Biol* 42(6):807–817.
44. Huffaker A, et al. (2013) Plant elicitor peptides are conserved signals regulating direct and indirect antiherbivore defense. *Proc Natl Acad Sci USA* 110(14):5707–5712.
45. Lampl N, Alkan N, Davydov O, Fluhr R (2013) Set-point control of RD21 protease activity by AtSerpin1 controls cell death in Arabidopsis. *Plant J* 74(3):498–510.
46. Rohrmeier T, Lehle L (1993) WIP1, a wound-inducible gene from maize with homology to Bowman-Birk proteinase inhibitors. *Plant Mol Biol* 22(5):783–792.
47. Shah J (2003) The salicylic acid loop in plant defense. *Curr Opin Plant Biol* 6(4):365–371.
48. Asai T, et al. (2000) Fumonisin B1-induced cell death in arabidopsis protoplasts requires jasmonate-, ethylene-, and salicylate-dependent signaling pathways. *Plant Cell* 12(10):1823–1836.
49. Doukhanina EV, et al. (2006) Identification and functional characterization of the BAG protein family in *Arabidopsis thaliana*. *J Biol Chem* 281(27):18793–18801.
50. Pennell RI, Lamb C (1997) Programmed cell death in plants. *Plant Cell* 9(7):1157–1168.
51. Christensen SA, Kolomiets MV (2011) The lipid language of plant-fungal interactions. *Fungal Genet Biol* 48(1):4–14.

Supplementary Figures, Tables and Datasets

Supplemental text	Supplemental Methods
Supplemental Figure S1	EI spectra of additional 9-LOX death acids
Supplemental Figure S2	Pathogen induced accumulation of candidate 9-LOX cyclopentenone pathway transcripts and 10-OPEA production in maize LOX mutants
Supplemental Figure S3	10-OPEA production in relation to α-ketols and chiral phase HPLC analysis of maize *cis*-10-OPEA
Supplemental Figure S4	Accumulation of DA^0-4:1, DA^0-4:0, and DA^0-2:0 following 10-OPEA application
Supplemental Figure S5	Levels of free linoleic acid and linolenic acids compared to 10-OPDA and derivatives
Supplemental Figure S6	Influence of subsequent tissue damage on phytohormones and DAs in control, wounded and SLB inoculated tissue
Supplemental Figure S7	Wound-induced accumulation 9-LOX cyclopentenones (10-OPEA and 10-OPDA) in sweet corn silks and herbivore induced 10-OPEA in maize stems
Supplemental Figure S8	Additional defense related-genes analyzed by RT-qPCR
Supplemental Figure S9	Time course of 10-OPEA induced ion leakage compared to related oxylipins, phytohormones and other controls.
Supplemental Figure S10	SLB induced lesions in leaves of HiII wild type and CC9-oe maize plants
Supplemental Table S1	NMR analysis of cyclopente(a)none oxylipins from maize
Supplemental Table S2	MapMan ontology based categorical enrichment of RNA-Seq groups
Supplemental Table S3	Genes investigated and primers used
Supplemental Dataset S1	Affymetrix GeneChip maize genome array investigating leaf 10-OPEA and control treatments at 90 minutes
Supplemental Dataset S2	Maize RNA-Seq leaf transcriptome changes mediated by 10-OPEA and 12-OPDA at 3 hours

Supplemental Materials and Methods

Plant, Insect, and Fungal Materials. Unless otherwise specified experiments were performed in the greenhouse using hybrid maize seed (*Zea mays* var. Golden Queen) grown under conditions as previously described (1). Hybrid sweet corn (var. Silver Queen and Peaches & Cream) was grown under summer field conditions in Tifton, GA following Ni et al. (2). Creation, growth and use of *ZmCC9* overexpression plants and respective HiII wild type controls were as previously described (3). Fungal stock cultures of *C. heterostrophus*, *A. flavus*, and *F. verticillioides* were grown on V8 agar for 1-3 weeks at 28°C at a 12/12 light/dark regime prior to experimental use in fungal suspensions (4, 5). For insect bioassays, *Helicoverpa zea* (Benzon Research, Inc. Carlisle, PA, USA) were received as late first instars, reared on artificial diet at 29°C, and utilized as early 3rd instars.

Maize Chemical Isolation and Quantification. Maize stem and inner whorl leaf tissue (4 kg) was excised, inoculated with SLB, and frozen 5 d post-treatment. Fungal infected tissue was ground to a powder in liquid N_2, extracted with 8L MeOH and filtered. MeOH was removed under vacuum and the remaining H_20 layer was acidified with HCl to pH 3, partitioned against 3L diethyl ether, collected and dried. The resulting oil was then separated by preparative flash chromatography (CombiFlash®R_f, Teledyne ISCO, Inc, Lincoln, NE, USA) on a 40 g Silica (RediSepRF Gold) column. The mobile phase followed from Weber et al. (6) and consisted of solvent A (hexane/acetic acid, 100:0.1) and solvent B (hexane/2-propanol /acetic acid, 70:30:0.1) with a continuous gradient of 0-30% B from 5 to 55 min using a flow rate of 40 ml min^{-1}. Over a range of 3-6% 2-propanol, a series of 9-LOX oxylipin enriched fractions were collected, dried under vacuum, and stored at -20^{o}C in EtOAc. Selected fractions were again separated by preparative flash chromatography (CombiFlash®R_f) on a 5 g C18 (RediSepRF Gold) column consisting of solvent A (H_20/acetonitrile, 90:10) and solvent B (acetonitrile/2-propanol, 95:5) with a continuous gradient of 0-100% B from 5 to 55 min using a flow rate of 40 ml min^{-1}. At each step, the content and

purity of all oxylipin fractions were analyzed as methyl esters by GC/MS. To achieve separation of *cis*/*trans* isomers and maximal purity for NMR, samples were derivatized with excess 2M (trimethylsilyl)diazomethane and subjected to HPLC using a Zorbax RX-silica (250 x 4.6 mm, 5 μm; Agilent) column with an isocratic mobile phase of 2-propanol /hexane (1:99, vol/vol) and a flow rate of 0.5 ml min^{-1} following Hamberg (7). This separation enabled the generation of pure *cis*-10-OPEA, *cis*-DA^0-4:1, *cis*-10-OPDA, *trans*-DA^1-4:0, *trans*-DA^1-2:0, *iso*-10-OPEA and *iso*-DA^0-4:0 as methyl esters. DA^0-4:0 and DA^0-2:0 were isolated as free acids by HPLC using a Zorbax RX-C18 (250 x 4.6 mm, 5 μm; Agilent) column and a mobile phase consisting of solvent A (H_20/formic acid, 100:0.1) and solvent B (2-propanol /formic acid, 100:0.1) with a continuous gradient of 10-80% B from 2 to 25 min using a flow rate of 1 ml min^{-1}. Purified fractions of DA^0-4:0 and DA^0-2:0 were collected between 16 and 18 min. For use in leaf toxicity assays, zealexin and kauralexin purification followed directly from established protocols (1, 5). For quantification of SA, jasmonates, and DAs described in this work, samples were solvent extracted, methylated, collected on a polymeric adsorbent using vapor-phase extraction (VPE), and analyzed using GC/isobutane CI-MS as previously described (1). Metabolite quantification was based on d_6-SA (Sigma-Aldrich, St. Louis, MO, USA), d_5-JA (C/D/N Isotopes Inc, Pointe-Claire, Canada), or U-^{13}C-18:3 (Cambridge Isotope Laboratories, Inc, Tewksbury, MA, USA), as internal standards. For α-ketol analysis, VPE was carried out with an additional silylation step, following trimethylsilyldiazomethane treatment and drying, by adding 30 µl of pyridine/hexamethyldisilazane/ trimethylchlorosilane at a ratio of 2:1:2 (v/v/v) at 25 °C for 20 min as described (36). GC/EI-MS quantification of the α-ketol, 9-hydroxy-10-oxo-12(Z)-octadecenoic acid (Larodan, Solna, Sweden), was based on an external curve using standard additions to untreated plant tissue samples. Chiral phase HPLC was performed with a Chiracel OB-H column (250 x 4.6mm; Diacel Chemical Industries, West Chester, PA, USA) using 2.75% 2-propanol in hexane as a mobile phase at a flow rate of 0.5ml/min with a diode-array detector at 220nm wavelength. Standards for racemic *cis*-10-OPEA, racemic *cis*-12-OPDA and

cis(+)-12-OPDA were purchased from Larodan (Solna, Sweden) and Cayman Chemical (Ann Arbor, MI, USA).

Interior whorl and silk treatments. For the comparison of local infection versus distal uninfected tissues, 28 d old plants were slit with a scalpel creating a centered parallel incision starting at the apical meristem and spanning a length of 5 cm upwards into the developing leaf tissues of the interior whorl. The incision site was then inoculated with 100 µl of 1 x 10^7 spores ml^{-1} of SLB as previously outlined (1). Local tissue was harvested by shaving the infected surface with a razor blade while 'distal' tissue was directly beneath this harvested layer and showed no visible signs of necrosis. For SLB infection involving subsequent crush damage treatments, 30 d old plants were injected 25 times (22 gauge needle) through the developing midribs every 0.5-1 cm spanning a distance from the apical node to the base of the whorl dispensing approximately 0.3 µl of SLB spore solution per injection. Damage controls were pierced in the same fashion with a 22 gauge needle containing H_20. Following inoculation and incubation periods, half of the treated region was harvested and frozen in liquid N_2. The other half was crush damaged by repeatedly rolling over the tissue with steel rod for 15 s followed by freezing in liquid N_2 at 30 min.

Fungal and insect growth bioassays. For anti-fungal bioassays, methods were performed as outlined in the Clinical and Laboratory Standards Institute M38-A2 guidelines following Schmelz et al. (1) with modifications including the use of 0.5% DMSO as the solvent control and a bioassay temperature of 26°C. To calculate fungal mass, *F. verticillioides*, *A. flavus*, and SLB suspensions with known $mg \cdot ml^{-1}$ concentrations were serially diluted and their optical density was measured at 405 nm to produce standard curves used to determine final amounts of fungal tissue following 72 h of growth. For insect growth inhibition trials, leaf whorl tissue was harvested from 30 day-old plants, ground with mortar and pestle in liquid N_2, then thawed for use as a diet base. Early 3rd-instar *H. zea* were allowed to feed on the leaf diet mixed with 0-750 $\mu g \cdot g^{-1}$ FW 10-OPEA for 24 h and then weighed for comparison against pre-treatment mass to

estimate growth. EtOH was used as a carrier for 10-OPEA and all control diets also contained a final concentration of 0.5% (v/w).

Cell Death and cytotoxicity Assays. For DNA laddering detection, the youngest leaf from 27 day-old plants was excised just above the apical meristem. Inner midrib tissue was isolated, sliced into 1.5 mm segments and placed in groups of 4 in a 24-well plate. Midrib segments were treated with 5 µl of 1-4mM 10-OPEA diluted in 1.875 µM NaOH buffer to pH 7, incubated at room temperature for 4 h, then harvested in liquid N_2. DNA extraction and laddering were performed following methods as previously described (8, 9). For cell death and cytotoxicity assays, the middle portion of individual emergent but not yet fully-expanded 4^{th} leaves were separately treated with two 10µl droplets of all test compounds at specified concentrations (often 2mM) dissolved in 5% DMSO and 0.1% Tween 20. At 24 h post treatment, lesion areas were photographed and digitally measured using ImageJ software (ImageJ 1.36b; Wayne Rasband, NIH, Bethesda, MD, USA). For ion leakage, the middle portion of the 4^{th} leaf was similarly treated with two 15 µl droplets of 2mM test compounds. At 2.5 h post treatment, 8mm dia. leaf discs encompassing the treatment area were excised, placed into 2.5 ml of H_2O and conductivity was measured as previously described (4).

Activity-Based Profiling with DCG-04 and Immunoblotting. For activity based protein profiling, 0.2 mg ml^{-1} of maize leaf extract was pre-incubated with 5 µM E-64 or control buffer for 30 min at room temperature. Following pre-incubation, Tris-HCl buffer (15 mM, pH=7.0) containing DTT (0.2 mM) and DCG-04 (2 mM) was added and samples were then incubated at room temperature for 3 h. Proteins were then precipitated with acetone and resolved in 2x Laemmli loading buffer (10). For immunoblotting, proteins were separated by SDS-PAGE followed by transfer to a nitrocellulose membrane. Biotinylated proteins were detected by streptavidin- horseradish peroxidase (1:3000) (Sigma-Aldrich, St. Louis, MO, USA) following van der Hoorn et al. (11)

Leaf treatments for transcript analysis. For gene expression analysis of SLB-infected leaves, spot inoculations were carried out by applying six 10 µl droplets of either 0.1% Tween 20 (control) or SLB suspension ($1x10^6$ spores ml^{-1}) onto the middle portion of partially emerged leaf 4 approximately 15 cm from the distal tip with three inoculation sites on each side of the midrib 2 cm apart. Following inoculation, plants were placed into a 100% humidity chamber. At 24 h post treatment, control and inoculated tissues were collected in liquid N_2. For chemical treatments, methods were performed as described above with the modification of using four 10µl droplets of 2mM compound (two droplets on either side of the midrib). For fungal and chemical leaf treatments, total RNA was isolated using the Nucleospin RNA Plant kit (Macherey-Nagel bmbH Inc., Duren, Germany) according to the manufacturers protocol and First Strand cDNA was synthesized using the Superscript III First Strand cDNA synthesis kit (Invitrogen, Carlsbad, CA, USA) with random decamer primers. qRT-PCR was performed with gene specific primers and normalized against the average of 2 control genes, *ZmUBCP* (GRMZM2G102471) and ZmFPGS (GRMZM2G393334) (*SI Appendix*, Table S3). Microarray analysis examining 10-OPEA activity at 90 min was carried out with Affymetrix (Santa Clara, CA, USA) GeneChip maize genome arrays using previously described methods (5) (Supplemental Dataset S1). For RNA-seq analysis of 10-OPEA and 12-OPDA treatments at 3 h**,** libraries were constructed using Illumina (San Diego, CA, USA) TruSeq Stranded RNA LT Kit following the manufacturer's instructions. The starting quantity of total RNA was adjusted to 1.3 µg, and all volumes were reduced to a third of the described quantity. Deep sequencing was performed using an Illumina NextSeq500 Instrument at the University of Georgia Genomics Facility.

RNA-Seq data analysis. Raw fastq reads were trimmed for adapters, preprocessed to remove low quality reads using Trimmomatic v0.32 (12). Sequencing of libraries was performed up to 75 cycles. Image analysis and base calling were performed with the standard Illumina pipeline**.** Qualified reads were then aligned to *Z. mays* AGPv3.25 reference genome using Bowtie2 v2.2.3.0 (13) and TopHat v2.0.13 (14). Gene expression values in to fragments per kilo base

per million reads (FPKM) were computed using Cufflinks v2.2.1 (15). Affymetrix maize genome arrays and RNA-Seq data generated for this work have been deposited in the NCBI Gene Expression Omnibus (GEO; http://www.ncbi.nlm.nih.gov/geo/) and are accessible through accession numbers GSE68589 and GSE69659, respectively. For statistical analyses, data were first filtered to remove all genes with zero counts across all twelve samples. Remaining gene FPKM were transformed by adding a small positive number (eight) prior to computing the logarithm base 2 following RNA-Seq Data Pathway and Gene-set Analysis Workflows (http://bioconductor.org). Statistical analysis was performed on these filtered-transformed data using the limma package version 3.22.7 (16), available through the R/Bioconductor project (http://www.R-project.org/) (17). A single-channel design was used to carry out the differential gene expression analysis (18). The function 'decideTest' with the global option was utilized to compute globally, FDR adjusted P-values to explore differences between the three treatment conditions (10-OPEA, 12-OPDA, control) across all genes (16, 19). The level of significance was set to 0.05. Supplemental Dataset S2 provides the gene identifications, the globally adjusted *P*-values associated with the statistically significant contrasts, and the adjusted means for each treatment groups. Supplemental Dataset S2 also includes MapMan bins, bin names, MapMan closest Arabidopsis match and Tair short description, the FPKM values across treatments and replicates, unadjusted FPKM means, and the sparkline graphical trend. To explore statistically significant ontology based categorical enrichment within the groups of similarly responding genes the data set was first filtered to remove all genes where no treatments resulted in any mean FPKM of greater than 1. This reduced reference genes from 30,538 to 18,155 and reduced the total number of significantly changing genes from 5276 to 4908. MapMan was used to assign BIN code ontologies to each annotated maize gene (20). R statistical computing software was used to determine significant over or under-representation of all MapMan bins that were present in each group of similarly responding genes (*SI Appendix*, Table S2). A hypergeometric test was performed for each MapMan bin present in each gene

group using the phyper-function from the statistical package. To account for the large number of comparisons the P-values were adjusted for each gene group separately using the p.adjust-function and a Benjamini Hockberg multiple testing correction (19).

References:

1. Schmelz EA, et al. (2011) Identity, regulation, and activity of inducible diterpenoid phytoalexins in maize. *Proc Natl Acad Sci USA* 108(13):5455-5460.
2. Ni X, et al. (2011) Spatial patterns of aflatoxin levels in relation to ear-feeding insect damage in pre-harvest corn. *Toxins* 3(7):920-931.
3. van der Linde K, et al. (2012) A maize cystatin suppresses host immunity by inhibiting apoplastic cysteine proteases. *Plant Cell* 24(3):1285-1300.
4. Huffaker A, Dafoe NJ, Schmelz EA (2011) ZmPep1, an ortholog of Arabidopsis Elicitor Peptide 1, regulates maize innate immunity and enhances disease resistance. *Plant Physiol.* 155(3):1325-1338.
5. Huffaker A, et al. (2011) Novel acidic sesquiterpenoids constitute a dominant class of pathogen-induced phytoalexins in maize. *Plant Physiol* 156(4):2082-2097.
6. Weber H, Vick BA, Farmer EE (1997) Dinor-oxo-phytodienoic acid: A new hexadecanoid signal in the jasmonate family. *Proc Natl Acad Sci USA* 94(19):10473-10478.
7. Hamberg M (2000) New cyclopentenone fatty acids formed from linoleic and linolenic acids in potato. *Lipids* 35(4):353-363.
8. Ryerson DE, Heath MC (1996) Cleavage of nuclear DNA into oligonucleosomal fragments during cell death induced by fungal infection or by abiotic treatments. *Plant Cell* 8(3):393-402.
9. Kim KS, Min J-Y, Dickman MB (2008) Oxalic acid is an elicitor of plant programmed cell death during Sclerotinia sclerotiorum disease development. *Mol. Plant. Microbe Interact.* 21(5):605-612.
10. Laemmli UK (1970) Cleavage of structural proteins during assembly of head of bacteriophage-T4. *Nature* 227(5259):680-685
11. van der Hoorn RAL, Leeuwenburgh MA, Bogyo M, Joosten M, Peck SC (2004) Activity profiling of papain-like cysteine proteases in plants. *Plant Physiol* 135(3):1170-1178.
12. Bolger AM, Lohse M, Usadel B (2014) Trimmomatic: a flexible trimmer for Illumina sequence data. *Bioinformatics* 30(15):2114-2120.
13. Langmead B, Salzberg SL (2012) Fast gapped-read alignment with Bowtie 2. *Nature Methods* 9(4):357-359.
14. Kim D, et al. (2013) TopHat2: accurate alignment of transcriptomes in the presence of insertions, deletions and gene fusions. *Genome Biol.* 14(4):R36
15. Trapnell C, et al. (2010) Transcript assembly and quantification by RNA-Seq reveals unannotated transcripts and isoform switching during cell differentiation. *Nat Biotechnol* 28(5):511-515.
16. Ritchie ME, et al. (2015) limma powers differential expression analyses for RNA-sequencing and microarray studies. *Nucleic Acids Res* 43(7):e47
17. Gentleman RC, et al. (2004) Bioconductor: open software development for computational biology and bioinformatics. *Genome Biol.* 5(10):R80

18. Smyth GK (2004) Linear models and empirical bayes methods for assessing differential expression in microarray experiments. *Stat Appl Genet Mol Biol* 3: Article 3.
19. Benjamini Y, Hochberg Y (1995) Controlling the false discovery rate - a practical and powerful approach to multiple testing. *Journal of the Royal Statistical Society Series B-Methodological* 57(1):289-300.
20. Usadel B, et al. (2009) A guide to using MapMan to visualize and compare Omics data in plants: a case study in the crop species, Maize. *Plant Cell and Environ* 32(9):1211-1229.

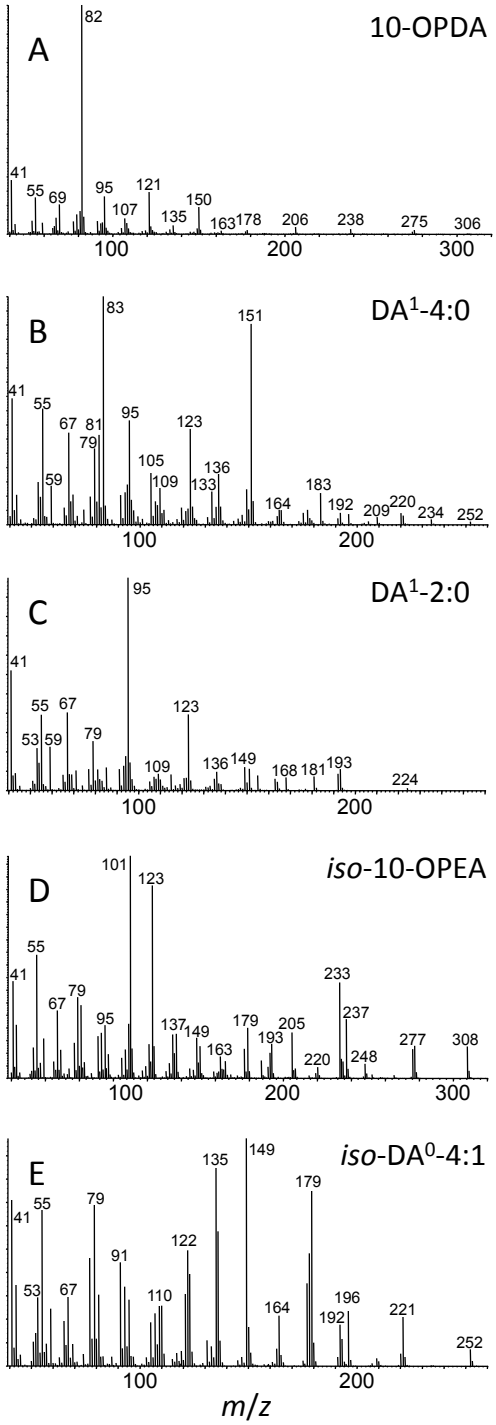

Fig. S1. GC/EI-MS spectra of additional DA series oxylipins as methyl ester derivatives. (*A*) 10-OPDA (*cis*) (10-oxo-11,15-phytodienoic acid methyl ester; (8-[(1, 5)-2-oxo-5-[(2)-pent-2-en-1-yl]cyclopent-3-en-1yl] octonic acid methyl ester) (*B*) DA^1-4:0 (*trans*) (4-[(1,5)-2-oxo-5-[(2)-pent-2-en-1-yl]clyclopentyl] butanoic acid methyl ester) (*C*) DA^1-2:0 (*trans*) (2-[(1,5)-2-oxo-5-[(2)-pent-2-en-1-yl]clyclopentyl] acetic acid methyl ester) (*D*) *iso*-10-OPEA (8-(5-oxo-2-pentylcyclopent-1-en-1-yl) octonic acid methyl ester) and (*E*) *iso*-DA^0-4:1 (4-(5-oxo-2-pentylcyclopent-1-en-1-yl) butanoic acid methyl ester).

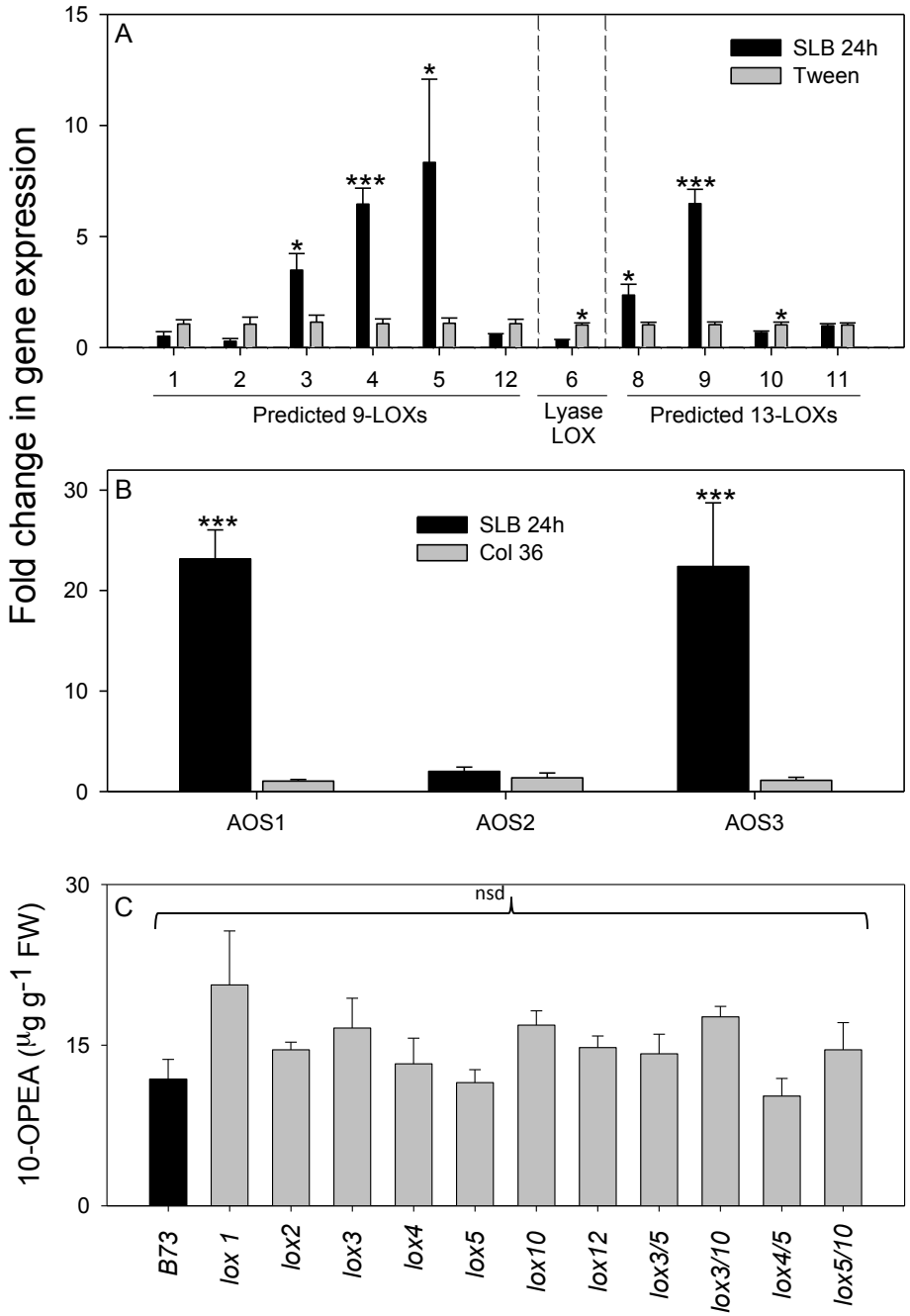

Fig. S2. Screening for candidate LOX and AOS DA biosynthetic genes in SLB-infected tissues. (*A*) Average (n = 4 ± SEM) qRT-PCR fold change in transcript levels of predicted 9-LOXs (LOX1, NM_001111533.1; LOX2, NM_001112503.1; LOX3, GRMZM2G109130; LOX4, GRMZM2G109056; LOX5, GRMZM2G102760; and LOX12 GRMZM2G106748), a LOX with lyase activity (LOX6, GRMZM2G040095), and predicted 13-LOXs (LOX8, GRMZM2G104843; LOX9, GRMZM2G017616; LOX10, GRMZM2G015419; and LOX11, GRMZM2G009479) 24 h post-infection with SLB. (*B*) Fold change in expression of AOS1 (GRMZM2G067225), AOS2 (GRMZM2G002178), and AOS3 (GRMZM2G376661) in response to SLB 24 h post-inoculation. (C) Screen of available SLB-infected single and double LOX mutants for a functional role in 10-OPEA production. Asterisks represent significant differences between SLB and Tween control treatments (ANOVA; * $P < 0.05$; ** $P < 0.01$; *** $P < 0.001$). The letters nsd indicate no significant differences.

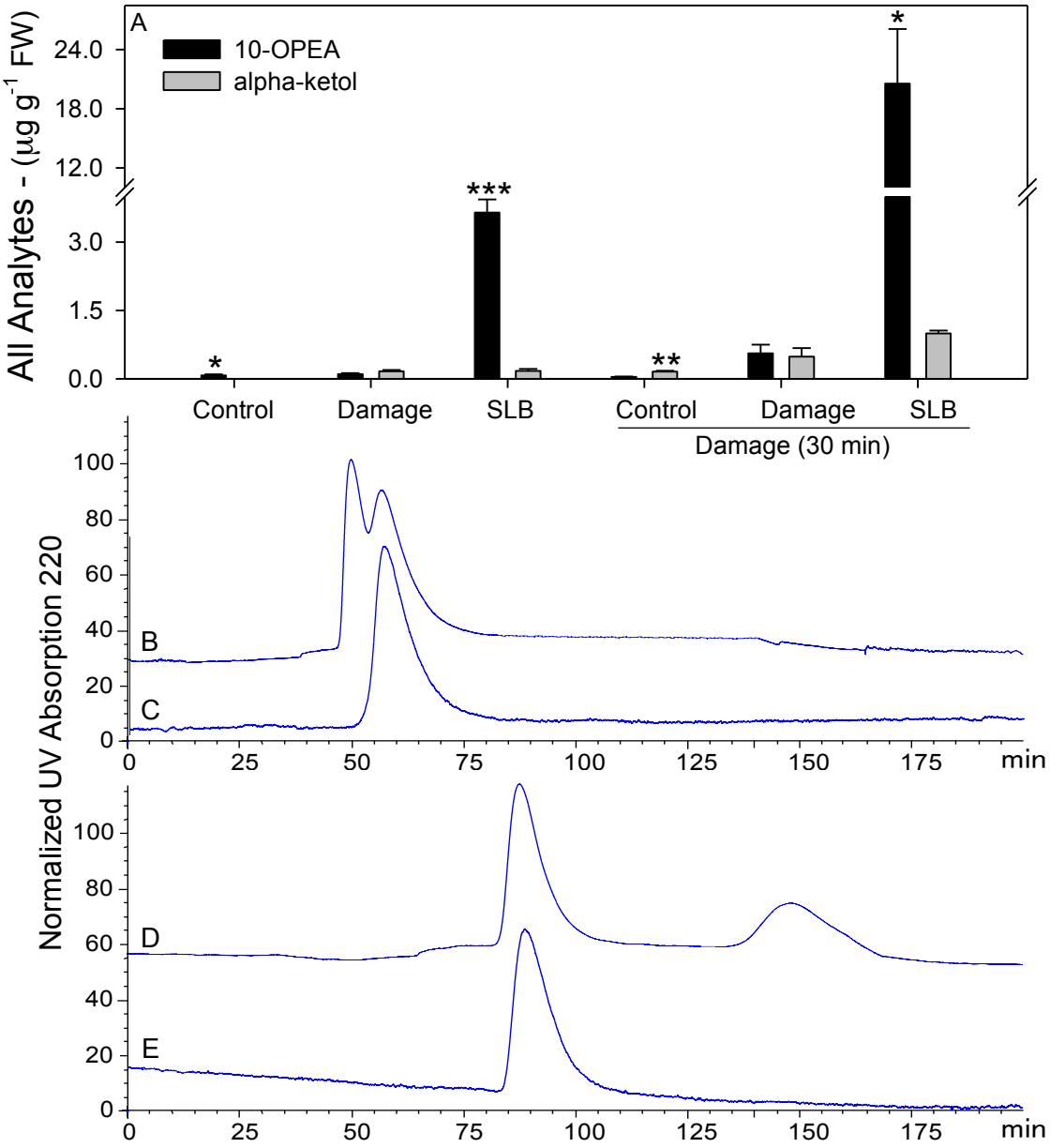

Fig. S3 Minimal α-ketol levels in SLB-infected tissues and a single *cis*-10-OPEA stereoisomer from wounded silks suggests enzymatic cyclization of 10-OPEA in maize. (A) Comparison of 10-OPEA and α-ketol concentrations in SLB infected maize tissue. 72 h post damage or SLB treatment, inner whorl tissues were either immediately harvested in liquid N_2 or crush-damaged and allowed to sit at room temperature for 30 m prior to collection. Levels of α-ketols (9-Hydroxy-10-oxo-12(*Z*)-octadecenoic acid) were analyzed by EI-GC/MS modified from Itoh et al. (2002). Asterisks represent significant differences between 10-OPEA and α-ketols for each treatment (ANOVA; * $P < 0.05$; ** $P < 0.01$; *** $P < 0.001$). (B-E) CP-HPLC was carried out with a Chiralcel OB-H column (250 x 4.6mm; Diacel Chemical Industries) using 2.75% isopropanol in hexane as the mobile phase at a flow rate of 0.5 ml/min. Chromatography of (B) racemic *cis* (+/-) 10-OPEA (Larodan) and (C) purified *cis*-10-OPEA from maize silk indicates the presence of a single predominant stereoisomer (one peak) compared to the two peaks observed in the commercial 1:1 mixture of *9R,13R* and *9S,13S* 10-OPEA. Similar results were observed using (D) a standard (Larodan) of racemic *cis*-(+/-)-12-OPDA where the 1:1 mixture of (*9R*,13*R*) and (9*S*,13*S*)-12-OPDA produced 2 peaks, while (E) *cis*-(*9S, 13S*)-12-OPDA (Cayman Chemical) produced a single peak.

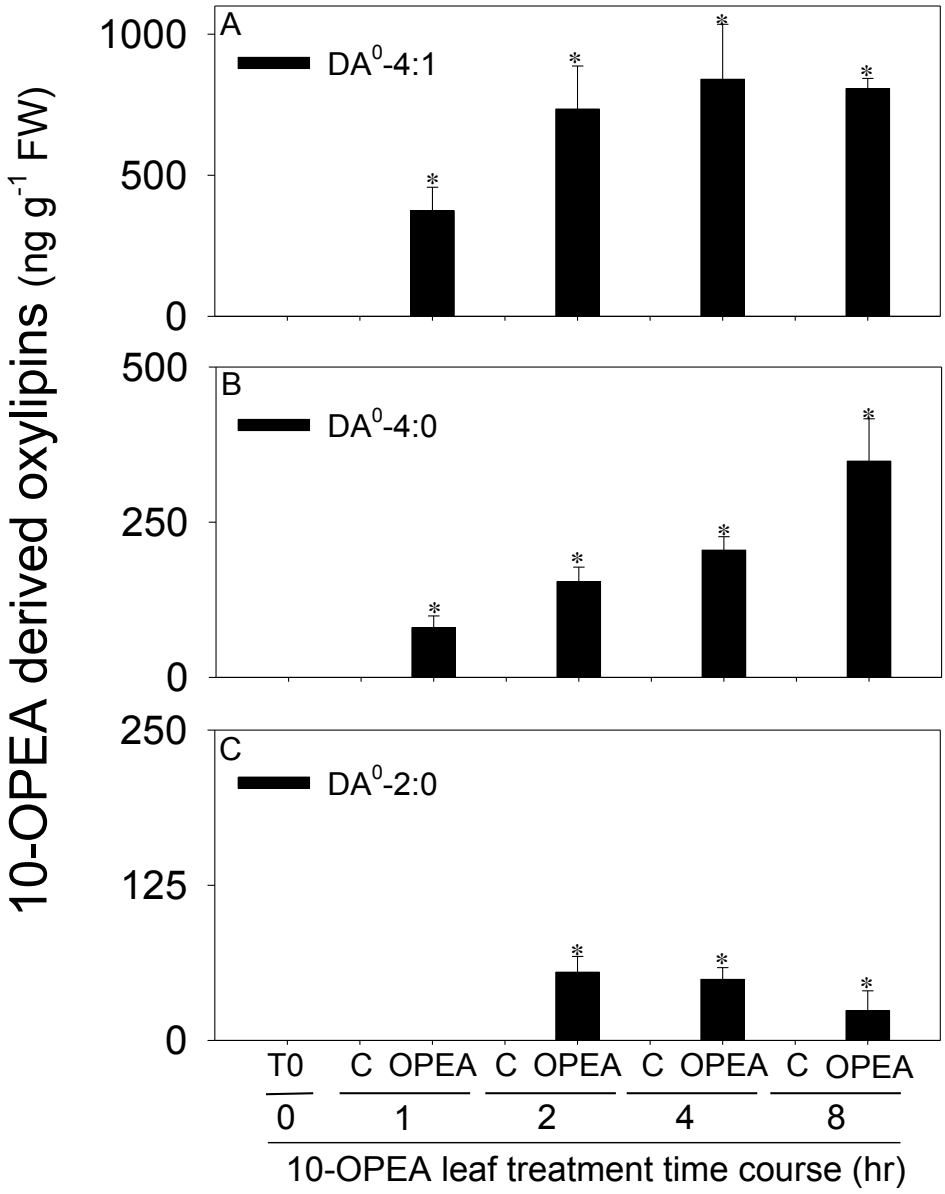

Fig. S4. Twelve and 14-carbon DAs rapidly accumulate following exogenous 10-OPEA leaf application. Average (n = 4, ± SEM) concentrations (ng g^{-1} FW) of (*A*) DA^0-4:1, (*B*) DA^0-4:0 and (*C*) DA^0-2:0 in emerging but not yet fully-expanded 4th leaves following treatment with four 10µl droplets of 2mM 10-OPEA or control solution (95:5:0.1 H_20:DMSO:Tween 20, v/v/v). At 1,2,4, and 8 h post-treatment, tissue was collected into liquid N_2 and oxylipin accumulation was accessed. Asterisk represents a significant difference between 10-OPEA treatment and control at each time point (ANOVA, $P<0.05$).

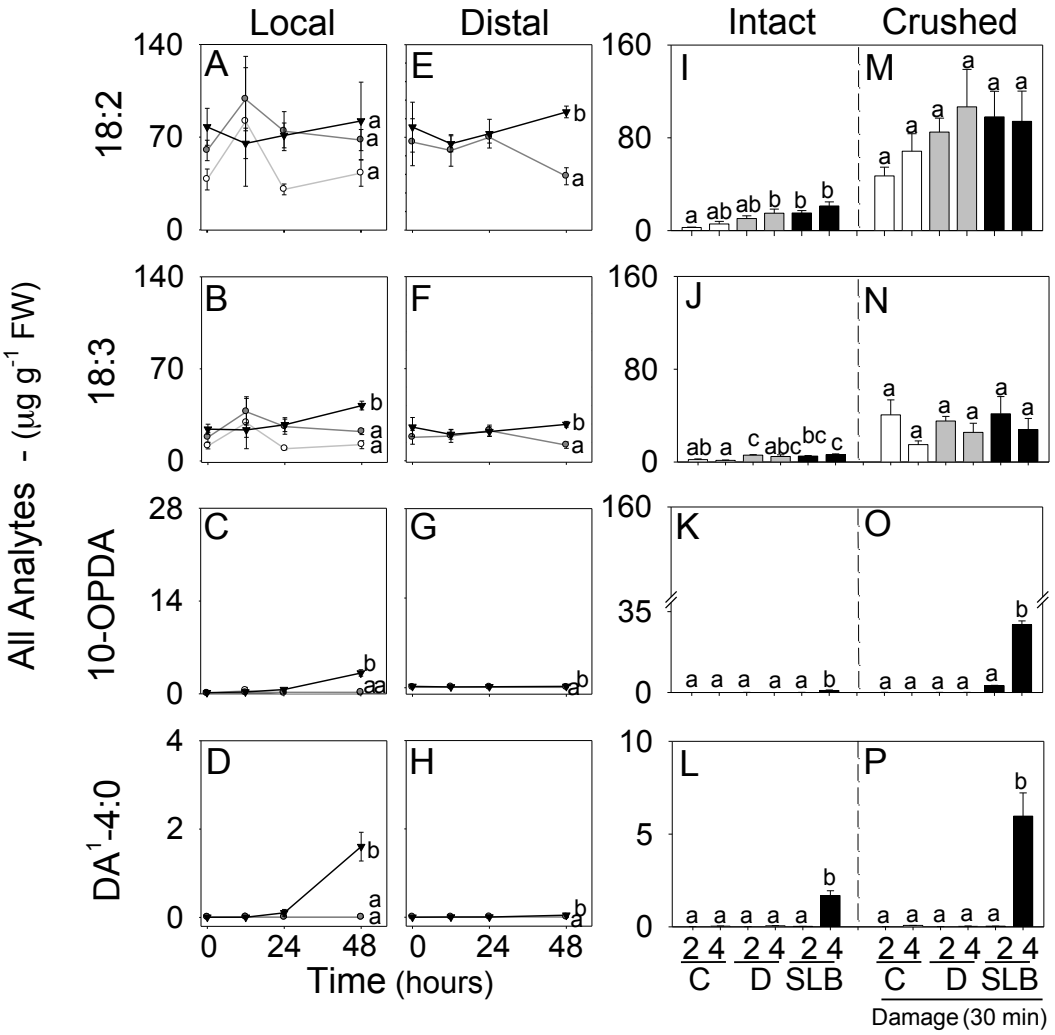

Fig. S5 Accumulation of fatty acids and 18:3 derived DAs in SLB infected tissue. Average (n = 4, ± SEM) concentrations (µg g^{-1} FW) of (*A, E*) 18:2, (*B, F*) 18:3, (*C, G*) 10-OPDA, and (*D, H*) DA^1-4:0 in maize interior whorl tissue following no treatment (open circle), mechanical incision damage (grey circle), and SLB inoculation (solid triangle). Two segments consisting of the infected site [Local; A-D] and visually asymptomatic tissue 1-2 mm adjacent to the treatment site [Distal; E-H] were collected for analysis at 0, 12, 24, and 48 h. Average (n = 4, ± SEM) concentrations (µg g^{-1} FW) of (*I, M*) 18:2, (*J, N*) 18:3, (*K, O*) 10-OPDA, and (*L, P*) DA^1-4:0 in interior whorl tissue following no treatment (white bars), mechanical damage (grey bars), and SLB inoculation (black bars) for 2 and 4 d. Tissues were immediately harvested intact (*I-L*) or were crushed (*M-P*) and allowed to sit for 30 min. Different letters (a-c) represent significant differences (P < 0.05 for Tukey test corrections for multiple comparisons).

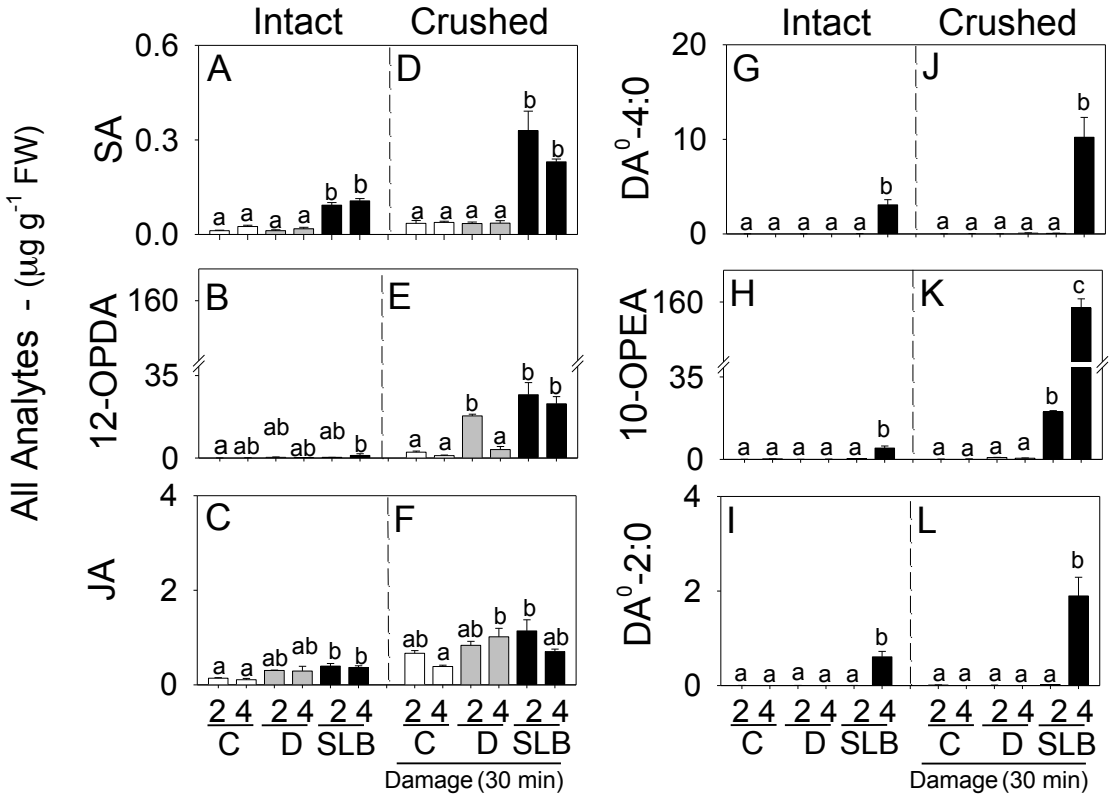

Fig. S6. DAs become wound-inducible in the context of pathogen attack. Average (*n* = 4, ± SEM) concentrations (µg g^{-1} FW) of (*A, D*) SA, (*B, E*) 12-OPDA, (*C, F*) JA, (*G, J*) DA^0-4:0, (*H, K*) 10-OPEA, and (*I, L*) DA^0-2:0 in interior whorl tissue following no treatment (white bars), mechanical damage (grey bars), and SLB inoculation (black bars) for 2 and 4 d. Tissues were immediately harvested intact (*A-C, G-I*) or were crushed (*D-F, J-L*) and allowed to sit for 30 min. Different letters (a-c) represent significant differences ($P < 0.05$ for Tukey test corrections for multiple comparisons).

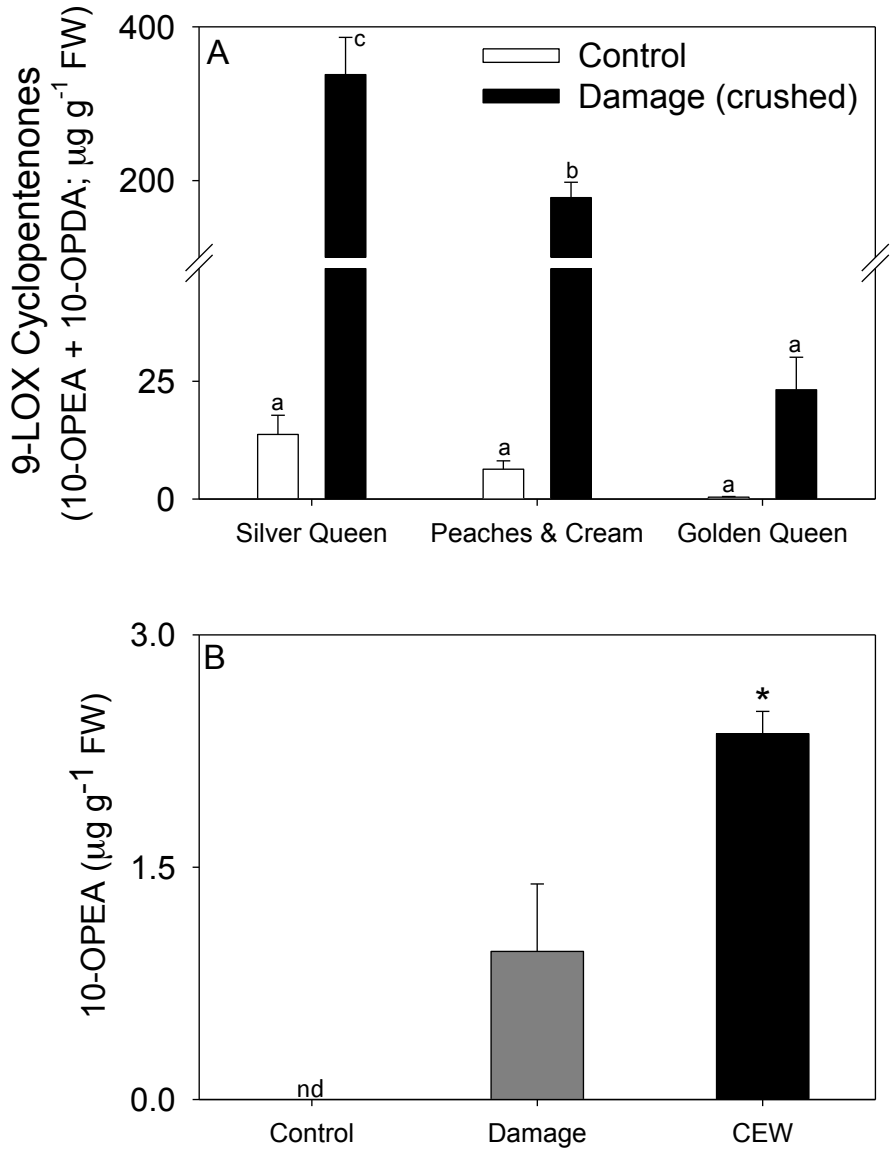

Fig. S7. Senescent sweet corn silks exhibit a large capacity for wound-induced accumulation of 9-LOX cyclopentenones while herbivore [corn earworm (CEW; *Helicoverpa zea*)] attack on stems results in comparatively modest 10-OPEA accumulation. (*A*) Average (n=4, ± SEM) 10-OPEA+10-OPDA (μg g^{-1} FW) levels in silks of different commercial sweet corn varieties. Silks were harvested 35 days after pollination from field grown (FG; *Zea mays* hybrids 'Silver Queen' and 'Peaches & Cream) and green house grown (GH; *Zea mays* hybrid 'Golden Queen') plants as intact controls or tissue subjected to crush damage (30 min) and subsequently snap frozen in N_2 for metabolite analysis. The ratio of 10-OPEA:10-OPDA for Silver Queen, Peaches and Cream, and Golden Queen is 4:1, 9:1, and 5:1, respectively. Different letters (a-c) represent significant differences (P < 0.05 for Tukey test corrections for multiple comparisons). (*B*) Average quantities (n=3, ± SEM) of 10-OPEA in maize interior whorl tissue following no treatment (control; white bar), damage (grey bars), or CEW infested stems (black bars). For infestation, a 3mm cork borer was used to create a hole at the apical meristem and 3rd instar CEW larvae were introduced into the hole and contained by securing a copper mesh over the infestation site. Tissue surrounding the cork borer site (damage) or from the tunnel feeding sites was collected 6 d post infestation. Asterisk represents a significant difference between CEW and damage treatments (ANOVA, P>0.05). The letters nd = not detected.

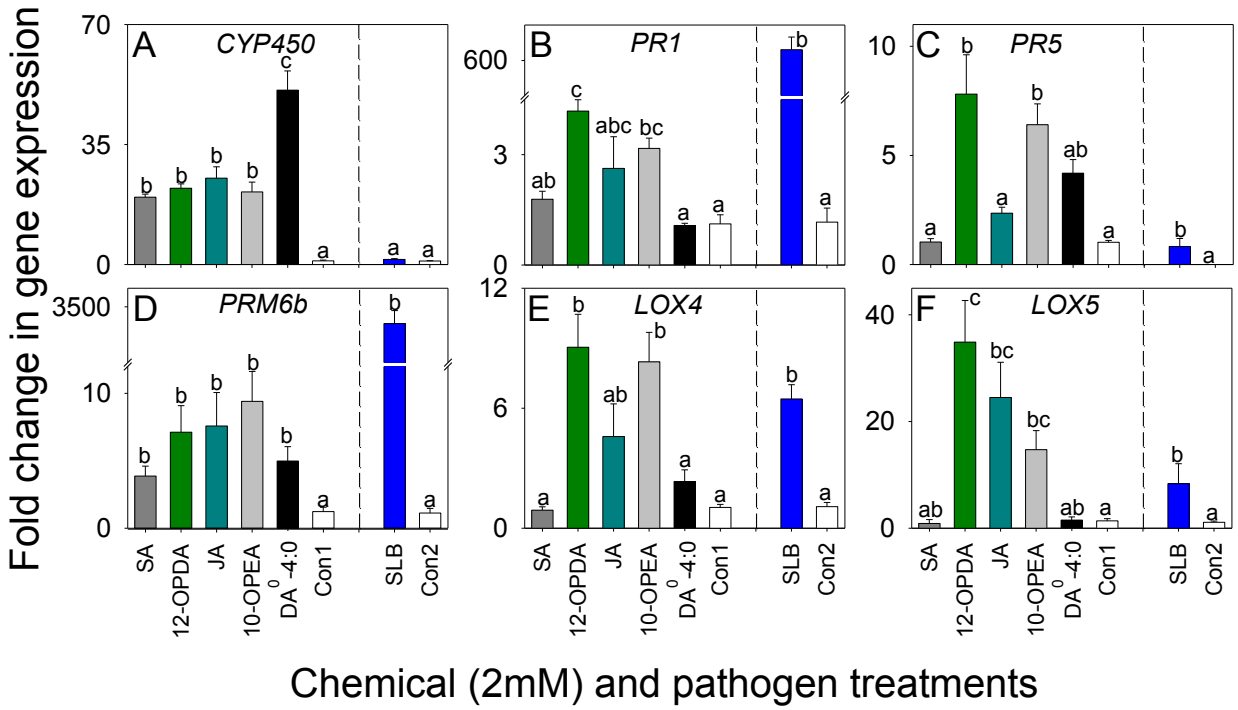

Fig. S8. 10-OPEA and DA^0-4:0 induce defense gene expression to levels comparable to other known plant defense hormones. Average (n = 4, ± SEM) qRT-PCR fold change in transcript levels of genes encoding defense proteins including (*A*) *CYP450*, (*B*) *ZmPR1*, (*C*) *ZmPR5*, (*D*) *ZmPRM6b*, (*E*) *ZmLOX4*, and (*F*) *ZmLOX5* 3h post treatment (all 2mM) with SA, 12-OPDA, JA, 10-OPEA, DA^0-4:0, or control solution (Con1: 95:5:0.1 H_20:DMSO:Tween 20, v/v/v); or 24 h post infection with SLB spores and H_20 with 0.1% Tween 20 (Con2). Within chemical and SLB infection treatment plots, different letters (a-c) represent significant differences (P < 0.05 for Tukey test corrections for multiple comparisons).

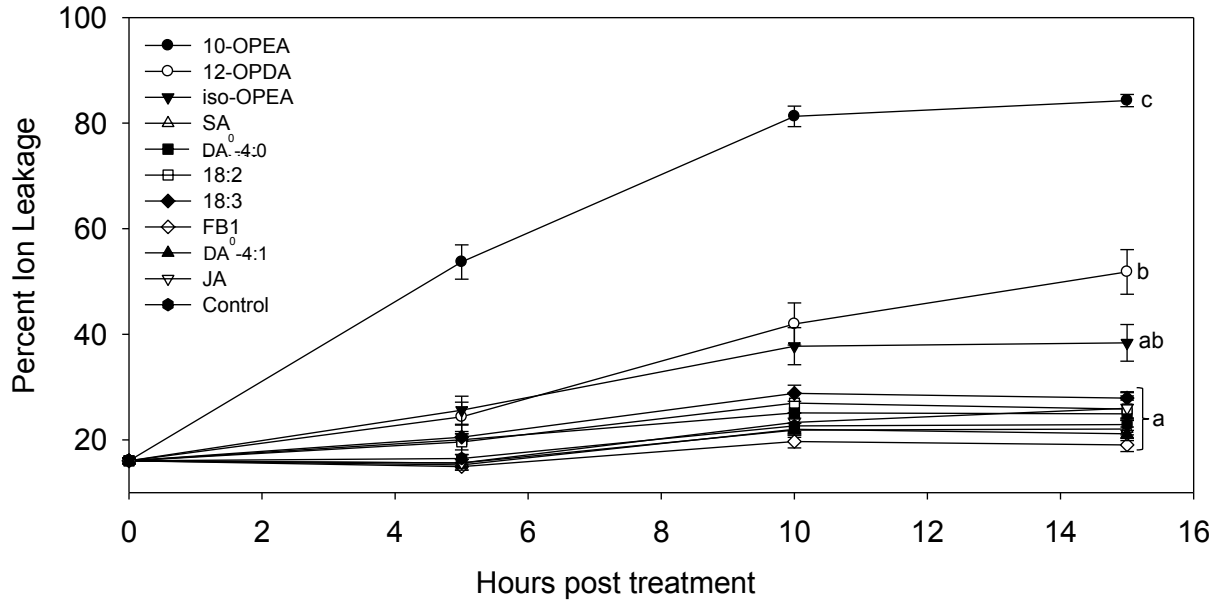

Fig. S9. 10-OPEA has strong cytotoxic effects producing ion leakage levels significantly higher than jasmonates, SA, fatty acids, and the common cell death-inducing mycotoxin fumonisin B1. Percent ion leakage was measured in µSiemens from leaf discs 5, 10, and 15 h post-treatment with 2mM 10-OPEA, 12-OPDA, *iso*-10-OPEA, salicylic acid (SA), DA^0-4:0, linoleic acid (18:2), linolenic acid (18:3), fumonison B1 (FB1), DA^0-4:1, jasmonic acid (JA), or control solution (95:5:0.1 H_20:DMSO:Tween 20, v/v/v). With the exceptions of 10-OPEA, 12-OPDA and *iso*-10-OPEA, all other treatments produced weak responses with overlapping or obscured plot symbols. Different letters (a-c) represent significant differences at the 15 h time point ($P < 0.05$ for Tukey test corrections for multiple comparisons).

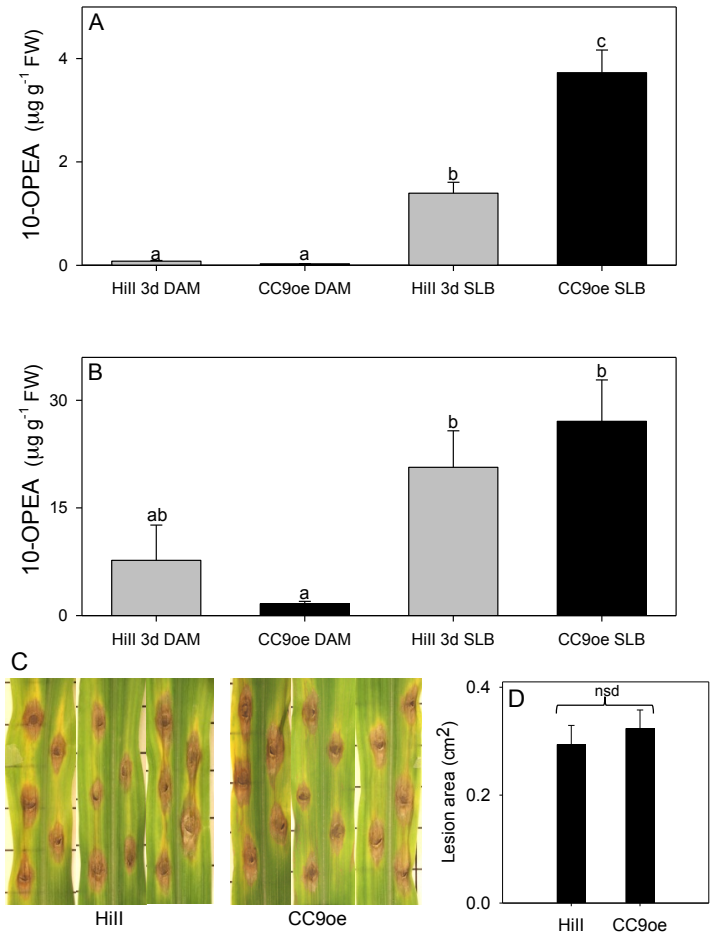

Fig. S10 Heightened 10-OPEA concentrations in CC9oe plants may restore SLB lesion areas to wild-type levels. (A-B), Average (*n* = 4, ± SEM) concentrations (µg g^{-1} FW) of 10-OPEA in wild-type HiII (grey bars) and CC9oe (black bars) interior whorl tissue following damage and SLB inoculation. Tissues were immediately harvested intact (*A*) or were crushed (*B*) and allowed to sit for 30 min. Different letters (a-c) represent significant differences ($P < 0.05$ for Tukey test corrections for multiple comparisons). (C-D), The 4^{th} leaf of HiII and CC9oe plants were inoculated with four 10ul droplets of SLB suspension ($1x10^6$) and placed in a humidity chamber for 24 hr. Following 24 h, plants were restored to normal green house conditions. 48 h post treatment, pictures were taken and lesions were measured with ImageJ software. The letters nsd indicate no significant difference (ANOVA, $P<0.05$).

General Experimental: All NMR data was acquired in $CDCl_3$ (Cambridge Isotope Laboratories, Inc.), 2.5-mm NMR tubes (Norell) at 22 °C using a 5-mm TXI cryoprobe (Bruker Corporation) and a Bruker Avance II 600 console (600 MHz for ^{1}H and 151 MHz for ^{13}C). 1D and 2D ^{1}H and ^{13}C NMR spectroscopy were used for structural elucidation. Relative stereochemistry was determined by GC retention times based on an authentic standard of predominantly cis-10-OPEA (Larodan; Malmö, Sweden). Residual $CHCl_3$ was used to reference chemical shifts to $\delta(CHCl_3)$ = 7.26 ppm for 1H and δ C of 77.36. NMR spectra were processed using Bruker Topspin 2.0 and MestReNova (Mestrelab Research) software packages. All compounds are numbered according to Hamberg (2000). In all figures COSY correlations are shown in red bonds and black arrows represent HMBC correlations.

Table S1.1. 10-oxo-11-phytoenoic acid (10-OPEA) methyl ester (*cis*) ^{1}H (600 MHz), ^{13}C (151 MHz), HSQC and HMBC NMR spectroscopic data in $CDCl_3$. Coupling constants are given in Hertz [Hz]. Selected HMBC correlations are shown in the figure.

Position	**δ ^{13}C [ppm]**	**δ ^{1}H [ppm]**	***J* coupling constants [Hz]**	**HMBC correlations (C. No)**
1	174.8	-	-	-
2	34.4	2H 2.30	t *J* = 7.6	C1, C3, C4
3	25.2	2H 1.62	m	C1, C2, C4
4 5 6	29.6	6H 1.32	m m m	-
7	28.3	2H 1.42	m	C6, C8, C9
8	25.8	1H 1.32 1H 1.69	m	C6, C9, C10, C13
9	50.2	1H 2.31	m	C10, C12, C13
10	212.1	-	-	-
11	132.9	1H 6.15	dd *J* = 5.8, 1.7	C9, C10, C13, C12, C14 (w)
12	167.5	1H 7.71	dd *J* = 5.8, 2.8	C9, C10, C11, C13, C14 (w)
13	44.6	1H 2.96	m	C10, C11, C12, C14
14	31.2	1H 1.13 1H 1.67	m	1.67- C13, C12, C15, C16
15	27.6	2H 1.33	m	-
16	32.4	2H 1.31	m	-
17	22.9	2H 1.31	p *J*= 7.5	-
18	14.3	3H 0.90	t *J* = 7.5	C16, C17
O-CH_3	51.8	3H 3.67	s	C1, C2 (w)

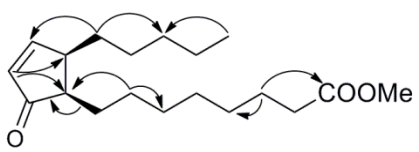

Table S1.2. DA^0-4:1 methyl ester (*cis*) (4-[(1, 5)-2-oxo-5-pentylcyclopent-3-ene-1-yl] hexanoic acid methyl ester) ^1H (600 MHz), ^{13}C (151 MHz), COSY, and HMBC NMR spectroscopic data in $CDCl_3$. Coupling constants are given in Hertz [Hz]. Selected HMBC and COSY correlations are shown in the figure.

Position	**δ ^{13}C [ppm]**	**δ ^1H [ppm]**	**J coupling constants [Hz]**	**HMBC correlations (C. No)**
1	173.98	-		
2	34.2	2H 2.37	m	C1, C3 (weak), C4 (weak)
3	23.86	2H 1.80	tdd *J*=12.5, 8.5, 5.9	C1 (weak), C2, C4
4	25.28	1H 1.39 1H 1.72	 m	1.72- C2 1.39- C3, C6, C5, C9
5	49.60	1H 2.32	m	C6, C4, C9
6	211.25	-	-	-
7	132.65	1H 6.16	dd *J* =5.9, 1.7	C6, C5, C8, C9
8	167.15	1H 7.75	dd *J*= 5.9, 2.8	C5, C9
9	44.30	1H 2.99	m	-
10	30.91	1H 1.70 1H 1.12	m dd *J*=13.2, 4.5	C5, C9
11	27.32	1H 1.40 1H 1.32	 m	-
12	32.07	2H 1.31	m	C13 weak
13	22.65	2H 1.32	m	C12
14	14.1	3H 0.90	t *J* = 6.9	C13, C12
O-CH3	51.70	3H 3.68	s	C1

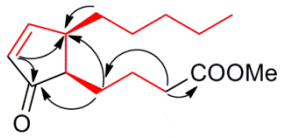

Table S1.3. DA^{0}-4:0 (*trans*) (4-[(1, 5)-2-oxo-5-pentylcyclopent-3-ene-1-yl] butanoic acid) ^{1}H (600 MHz), ^{13}C (151 MHz), COSY, HMBC, NOESY NMR spectroscopic data in $CDCl_3$. Coupling constants are given in Hertz [Hz]. Selected HMBC and COSY correlations are shown in the figure.

Position	**δ ^{13}C [ppm]**	**δ ^{1}H [ppm]**	**J coupling constants [Hz]**	**HMBC correlations (C. No)**
1	176.2	-		
2	33.7	2H 2.37	m	C1, C3, C4
3	22.1	1H 1.59 1H 1.78	m	1.59- C1 1.78- C1, C2, C4
4	27.3	2H 1.59	m	C3, C9, C6, C5
5	55.0	1H 1.71	m	C3, C4, C6
6	221.4	-	-	-
7	37.9	1H 2.34 1H 2.07	2.34 br t J= 9.4	2.34- C6, C9 2.07- C6
8	27.1	1H 2.15 1H 1.38	m	2.15- C6, C7, C5
9	41.8	1H 1.82	m	C5, C10
10	26.9	1H 1.42 1H 1.29	m	-
11	34.7	1H 1.66 1H 1.25	m	1.25- C10, C13
12	32.1	2H 1.30	m	-
13	22.7	2H 1.32	m	-
14	14.1	3H 0.90	t *J* = 7.0	C13, C12

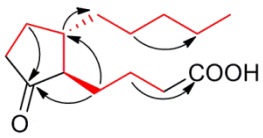

Table S1.4. DA^{0}-2:0 (*trans*) (2-[(1, 5)-2-oxo-5-pentylcyclopent-3-ene-1-yl] acetic acid) ^{1}H (600 MHz), ^{13}C (151 MHz), COSY, HMBC, spectroscopic data in $CDCl_3$. Coupling constants are given in Hertz [Hz]. Selected COSY and HMBC correlations are shown in the figure.

Position	**δ ^{13}C [ppm]**	**δ ^{1}H [ppm]**	***J* coupling constants [Hz]**	**HMBC correlations (C. No)**
1	174.9	-	-	-
2	32.2	2H 2.63	dd *J*= 5.4, 2.5	C1, C3, C4, C7
3	51.9	1H 2.11	dd *J*=11.7,5.7	C1 (w), C7, C8
4	220.3	-		
5	37.4	1H 2.23 1H 2.41	m	2.41- C4, C6, C7
6	27.1	1H 1.43 1H 2.22	m	1.43- C3, C4, C5, C7, C9
7	42.1	1H 1.91	br m	-
8	26.8	1H 1.29 1H 1.44	m	-
9	34.4	1H 1.66 1H 1.29	m	1.66- C7, C8, C10
10	32.1	2H 1.29	m	-
11	22.7	2H 1.32	m	-
12	14.3	3H 0.90	t J = 6.9	C11, C10

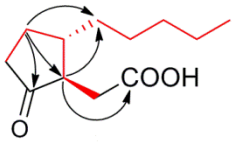

Table S1.5. 10-oxo-11,15-phytodienoic acid methyl ester (*cis*) (8-[(1, 5)-2-oxo-5-[(2)-pent-2-en-1-yl]cyclopent-3-en-1yl] octonic acid methyl ester) ^{1}H (600 MHz), ^{13}C (151 MHz), COSY, and HMBC NMR spectroscopic data in $CDCl_3$. Coupling constants are given in Hertz [Hz]. Selected HMBC and COSY correlations are shown in the figure.

Position	δ ^{13}C [ppm]	δ ^{1}H [ppm]	J coupling constants [Hz]	HMBC correlations (C. No)
1	175.5	-		
2	35.2	2H 2.30	t *J* = 7.6	C1, C3, C4
3	26.0	2H 1.61	m	C1, C2, C4
4 5 6	30.3	6H 1.32	m m m	- - -
7	29.5	2H 1.45	m	C6, C8, C9
8	26.8	1H 1.36 1H 1.72	m	C7, C9, C10, C13
9	50.6	1H 2.33	m	C7, C8, C10, C13
10	212.7	-	m	-
11	133.8	1H 6.16	dd *J* = 5.8, 1.7	C9, C10, C13, C12
12	168.1	1H 7.64	dd *J* = 5.8, 2.8	C9, C10, C11, C13
13	45.5	1H 3.01	m	C9, C10, C11, C12, C14, C15
14	29.6	1H 1.93 1H 2.37	m	1.93- C9, C13, C12, C15, C16 2.37- C13, C12, C15, C16
15	126.8	1H 5.36	m	C13, C14, C16, C17
16	135.3	1H 5.49	m	C14, C15, C17, C18
17	21.8	2H 2.00	p *J*= 7.5	C16, C15, C18
18	15.1	3H 0.95	t J = 7.5	C16, C17
O-CH_3	52.6	3H 3.66	s	C1

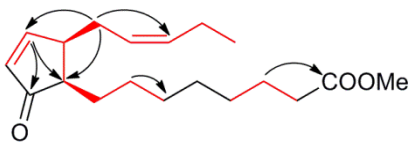

Table S1.6. DA[1]-4:0 methyl ester (*trans*) (4-[(1,5)-2-oxo-5-[(2)-pent-2-en-1-yl]clyclopentyl] butanoic acid methyl ester) ^{1}H (600 MHz), ^{13}C (151 MHz), COSY, and HMBC NMR spectroscopic data in $CDCl_3$. Coupling constants are given in Hertz [Hz]. Selected HMBC and COSY correlations are shown in the figure.

Position	δ ^{13}C [ppm]	δ ^{1}H [ppm]	J coupling constants [Hz]	HMBC correlations (C. No)
1	174.3	-		
2	34.5	2H 2.32	m	C1, C3, C4
3	22.5	1H 1.77 1H 1.58	m	1.58- C1, C4 1.77- C1, C2, C4
4	27.8	1H 1.58	m	C2, C3, C5, C6, C9
5	54.5	1H 1.77	m	C6, C4, C3, C10
6	221.1	-		
7	38.0	1H 2.08 1H 2.32	m	2.08- C8 2.32-C6, C9
8	26.9	1H 1.44 1H 2.10	m	1.44- C6, 2.10- C6, C5, C9, C11 (w), C12 (w)
9	42.0	1H 1.91	m	-
10	31.8	1H 2.08 1H 2.36	m	2.36- C5, C8, C9, C11, C12
11	126.1	1H 5.36	m	C9, C10, C12, C13
12	134.2	1H 5.48	m	C10, C11, C13, C14
13	21.0	2H 2.05	m	C11, C12, C14
14	14.6	3H 0.97	t J = 7.5	C13, C12
O-CH3	51.8	3H 3.66	s	C1

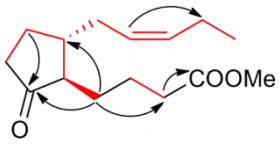

Table S1.7. DA[1]-2:0 methyl ester (*trans*) (2-[(1,5)-2-oxo-5-[(2)-pent-2-en-1-yl]clyclopentyl] acetic acid methyl ester) ^{1}H (600 MHz), ^{13}C (151 MHz), COSY, HMBC, NMR spectroscopic data in $CDCl_3$. Coupling constants are given in Hertz [Hz]. COSY (red) and key HMBC correlations are shown in the figure below.

Position	**δ ^{13}C [ppm]**	**δ ^{1}H [ppm]**	**J coupling constants [Hz]**	**HMBC correlations (C. No)**
1	172.69	-	-	
2	32.42	2H 2.63	dd *J*= 5.2, 1.8	C1, C3, C4, C7
3	51.30	1H 2.12	m	C4 (weak)
4	219.04	-		
5	37.38	1H 2.23 1H 2.37	m	2.23- C4 2.37-, C4, C7
6	27.12	1H 1.46 1H 2.15	m	1.46- C5, C7 (weak), C8 (weak)
7	41.90	1H 2.0	m	
8	31.5	1H 2.32 1H 2.11	m	2.11- C9 2.32- C9
9	125.73	1H 5.35	m	C8, C10
10	134.05	1H 5.48	m	C8, C9, C11, C12
11	20.74	2H 2.04	m	C9, C12
12	14.26	3H 0.96	t *J* = 7.5	C11, C10
O-CH3	51.87	3H 3.67	s	C1

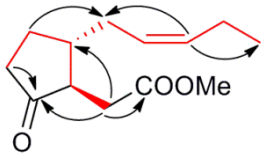

Table S1.8. *iso*-10-OPEA methyl ester (8-(5-oxo-2-pentylcyclopent-1-en-1-yl) octonic acid methyl ester) ^{1}H (600 MHz), ^{13}C (151 MHz), COSY, and HMBC NMR spectroscopic data in $CDCl_3$. Coupling constants are given in Hertz [Hz]. Selected HMBC and COSY correlations shown in the figure.

Position	δ ^{13}C [ppm]	δ ^{1}H [ppm]	J coupling constants [Hz]	HMBC correlations (C. No)
1	174.5	-		
2	34.2	2H 2.29	t J = 7.6	C1, C3, C4
3	25.0	2H 1.60	m	C1 (weak), C2, C4
4	29.3	6H 1.28	m	-
5			m	-
6			m	-
7	28.7	2H 1.34	m	C6 (w)
8	23.2	2H 2.14	t *J* = 7.6	C7, C9, C10, C13,
9	140.6	-	m	-
10	210.4	-	m	-
11	34.4	2H 2.35	m	C10, C12, C13
12	29.1	2H 2.48	m	C9, C10, C11, C13, C14
13	174.3	-	m	
14	31.3	2H 2.39	t *J* = 7.8	C9, C12, C13 C15, C16
15	27.3	2H 1.52	m	C13, C16, C17
16	32.0	2H 1.32	m	C17
17	22.5	2H 1.33	m	C16
18	14.0	3H 0.91	t *J* = 7.0	C16, C17
O-CH_3	51.6	3H 3.66	s	C1

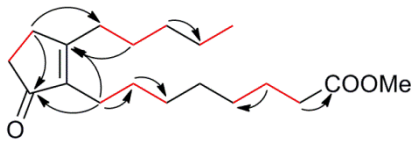

Table S1.9. *iso*-DA^0-4:1 methyl ester (4-(5-oxo-2-pentylcyclopent-1-en-1-yl) butanoic acid methyl ester) ^{1}H (600 MHz), ^{13}C (151 MHz), COSY, HMBC, NOESY NMR spectroscopic data in $CDCl_3$. Coupling constants are given in Hertz [Hz]. Selected HMBC and COSY correlations are shown in the figure.

Position	δ ^{13}C [ppm]	δ ^{1}H [ppm]	J coupling constants [Hz]	HMBC correlations (C. No)
1	174.10	-		
2	33.8	2H 2.29	t *J* = 7.4	C1, C3, C4
3	23.79	2H 1.71	tt *J*= 9.4,6.8	C1, C2, C4, C5
4	22.47	2H 2.20	t *J* = 7.7	C1, C2, C3, C5, C6
5	139.55	-	-	-
6	210.14	-	-	-
7	34.32	2H 2.36	m	C6, C9
8	29.11	2H 2.50	m	C5, C6, C7,C9, C10
9	174.26	-	m	-
10	31.28	2H 2.41	br t *J*= 7.8	C8, C9, C5, C11, C12
11	27.30	2H 1.52	m	C9, C12, C13
12	32.0	2H 1.32	t *J* = 7.8	C13
13	22.47	2H 1.33	m	C12, C14
14	14.0	3H 0.91	t *J* = 7.0	C12, C13
O-CH_3	51.6	3H 3.66	s	C1

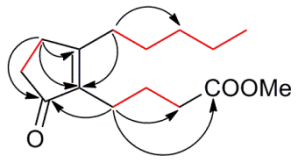

Table S2: MapMan ontology based categorical enrichment of cyclopentenone responsive co-regulated gene transcripts

MapMan BIN codes Group 1 [10-OPEA (+), 12-OPDA (++), Control (0)]	P-Value	Adjusted P-Value	Fold Enrichment	Enrichment Direction
13.1.6 - amino acid metabolism.synthesis.aromatic aa	1.12E-19	3.47E-17	11.47	Over
13.1.6.1 - amino acid metabolism.synthesis.aromatic aa.chorismate	7.54E-13	1.17E-10	19.28	Over
13.1 - amino acid metabolism.synthesis	1.32E-11	1.36E-09	4.44	Over
16 - secondary metabolism	5.65E-11	4.37E-09	3.84	Over
13 - amino acid metabolism	1.99E-10	1.23E-08	3.56	Over
35 - not assigned	3.08E-09	1.36E-07	0.71	Under
35.2 - not assigned.unknown	3.08E-09	1.36E-07	0.71	Under
17 - hormone metabolism	4.06E-09	1.57E-07	3.24	Over
17.7.1 - hormone metabolism.jasmonate.synthesis-degradation	2.47E-08	8.48E-07	11.83	Over
17.7 - hormone metabolism.jasmonate	8.05E-08	2.49E-06	10.51	Over
29.2 - protein.synthesis	1.00E-07	2.82E-06	0.05	Under
13.1.6.5 - amino acid metabolism.synthesis.aromatic aa.tryptophan	1.15E-07	2.96E-06	10.14	Over
13.1.6.5.1 - amino acid metabolism.synthesis.aromatic aa.tryptophan.anthranilate synthase	1.60E-06	3.81E-05	19.72	Over
29.2.1 - protein.synthesis.ribosomal protein	1.69E-05	0.00037	0.08	Under
16.2 - secondary metabolism.phenylpropanoids	6.73E-05	0.00139	4.03	Over
2 - major CHO metabolism	8.67E-05	0.00167	3.64	Over
2.2.1 - major CHO metabolism.degradation.sucrose	0.00010	0.00177	6.13	Over
17.4.1 - hormone metabolism.cytokinin.synthesis-degradation	0.00011	0.00177	14.02	Over
34 - transport	0.00011	0.00177	1.74	Over
17.7.1.3 - hormone metabolism.jasmonate.synthesis-degradation.allene oxidase synthase	0.00012	0.00190	23.66	Over
17.5.1 - hormone metabolism.ethylene.synthesis-degradation	0.00015	0.00221	7.01	Over
16.4.1 - secondary metabolism.N misc.alkaloid-like	0.00017	0.00243	12.62	Over
29.4.1.57 - protein.postranslational modification.kinase.receptor like cytoplasmatic kinase VII	0.00021	0.00283	3.54	Over
16.8.1 - secondary metabolism.flavonoids.anthocyanins	0.00030	0.00383	18.93	Over
17.4 - hormone metabolism.cytokinin	0.00038	0.00475	7.51	Over
29.4.1 - protein.postranslational modification.kinase	0.00052	0.00617	2.98	Over
13.1.6.1.5 - amino acid metabolism.synthesis.aromatic aa.chorismate.shikimate kinase	0.00058	0.00659	15.77	Over
27.1 - RNA.processing	0.00072	0.00792	0.11	Under
2.2 - major CHO metabolism.degradation	0.00080	0.00795	3.88	Over
34.9 - transport.metabolite transporters at the mitochondrial membrane	0.00088	0.00795	3.82	Over
10.1 - cell wall.precursor synthesis	0.00088	0.00795	4.33	Over
17.2.1 - hormone metabolism.auxin.synthesis-degradation	0.00098	0.00795	13.52	Over
8.1.4 - TCA / org. transformation.TCA.IDH	0.00098	0.00795	13.52	Over
16.8 - secondary metabolism.flavonoids	0.00099	0.00795	4.25	Over
16.1.1.5 - secondary metabolism.isoprenoids.non-mevalonate pathway.MCS	0.00100	0.00795	31.54	Over
13.1.6.1.10 - amino acid metabolism.synthesis.aromatic aa.chorismate.dehydroquinate/shikimate dehydrogenase	0.00100	0.00795	31.54	Over
13.1.6.1.2 - amino acid metabolism.synthesis.aromatic aa.chorismate.3-dehydroquinate synthase	0.00100	0.00795	31.54	Over
17.7.1.4 - hormone metabolism.jasmonate.synthesis-degradation.allene oxidase cyclase	0.00100	0.00795	31.54	Over
16.2.1.2 - secondary metabolism.phenylpropanoids.lignin biosynthesis.C4H	0.00100	0.00795	31.54	Over
16.4 - secondary metabolism.N misc	0.00124	0.00957	7.89	Over
10.1.5 - cell wall.precursor synthesis.UXS	0.00151	0.01140	11.83	Over
30.2.24 - signalling.receptor kinases.S-locus glycoprotein like	0.00157	0.01155	7.42	Over
16.1 - secondary metabolism.isoprenoids	0.00164	0.01176	3.15	Over
17.7.1.2 - hormone metabolism.jasmonate.synthesis-degradation.lipoxygenase	0.00220	0.01508	10.51	Over
23.4.1 - nucleotide metabolism.phosphotransfer and pyrophosphatases.adenylate kinase	0.00220	0.01508	10.51	Over
30.2 - signalling.receptor kinases	0.00272	0.01796	2.09	Over
27 - RNA	0.00273	0.01796	0.75	Under
17.8 - hormone metabolism.salicylic acid	0.00304	0.01916	9.46	Over
17.8.1 - hormone metabolism.salicylic acid.synthesis-degradation	0.00304	0.01916	9.46	Over
29 - protein	0.00318	0.01967	0.79	Under
16.1.1 - secondary metabolism.isoprenoids.non-mevalonate pathway	0.00411	0.02490	5.74	Over
28 - DNA	0.00491	0.02876	0.29	Under
26.28 - misc.GDSL-motif lipase	0.00493	0.02876	4.26	Over
11.8.2 - lipid metabolism.exotics (steroids, squalene etc).methylsterol monooxygenase	0.00565	0.03115	15.77	Over
13.1.6.4 - amino acid metabolism.synthesis.aromatic aa.tyrosine	0.00565	0.03115	15.77	Over
13.1.6.4.1 - AA metabolism.synthesis.aromatic AA.tyrosine.arogenate & prephenate dehydrogenase	0.00565	0.03115	15.77	Over
28.1 - DNA.synthesis/chromatin structure	0.00600	0.03252	0.14	Under
26 - misc	0.00620	0.03302	1.44	Over
27.3.4 - RNA.regulation of transcription.ARF, Auxin Response Factor family	0.00646	0.03381	5.05	Over
26.7 - misc.oxidases - copper, flavone etc.	0.00705	0.03629	3.32	Over
33.1 - development.storage proteins	0.00811	0.04022	6.76	Over
27.3.3 - RNA.regulation of transcription.AP2/EREBP, APETALA2/Ethylene-responsive element binding protein family	0.00883	0.04022	3.15	Over
13.1.1.2 - amino acid metabolism.synthesis.central amino acid metabolism.aspartate	0.00911	0.04022	12.62	Over
13.1.1.2.1 - amino acid metabolism.synthesis.central amino acid metabolism.aspartate.aspartate aminotransferase	0.00911	0.04022	12.62	Over
22.1.6 - polyamine metabolism.synthesis.spermidine synthase	0.00911	0.04022	12.62	Over
13.1.6.2.1 - amino acid metabolism.synthesis.aromatic aa.phenylalanine and tyrosine.chorismate mutase	0.00911	0.04022	12.62	Over
13.1.6.1.1 - AA metabolism.synthesis.aromatic AA.chorismate.3-deoxy-D-arabino-heptulosonate 7-phosphate syn	0.00911	0.04022	12.62	Over
34.23 - transport.hormones	0.00911	0.04022	12.62	Over
34.23.1 - transport.hormones.auxin	0.00911	0.04022	12.62	Over
2.2.1.5 - major CHO metabolism.degradation.sucrose.Susy	0.00911	0.04022	12.62	Over
2.2.1.3 - major CHO metabolism.degradation.sucrose.invertases	0.00982	0.04272	6.31	Over
10 - cell wall	0.01041	0.04469	1.93	Over
17.5 - hormone metabolism.ethylene	0.01164	0.04926	2.96	Over

Table S2: MapMan categorical enrichment (continued)				
MapMan BIN codes Group 2 [10-OPEA (0), 12-OPDA (+), Control (0)]	**P-Value**	**Adjusted P-Value**	**Fold Enrichment**	**Enrichment Direction**
10 - cell wall	2.15E-06	0.00055	3.46	Over
10.2 - cell wall.cellulose synthesis	5.12E-06	0.00066	7.95	Over
26.10 - misc.cytochrome P450	3.97E-05	0.00342	4.31	Over
10.2.2 - cell wall.cellulose synthesis.COBRA	6.65E-05	0.00429	29.08	Over
34 - transport	8.53E-05	0.00440	1.85	Over
26 - misc	0.00094	0.04052	1.68	Over
35 - not assigned	0.00153	0.04936	0.86	Under
35.2 - not assigned.unknown	0.00153	0.04936	0.86	Under
MapMan BIN codes Group3 [10-OPEA (-), 12-OPDA (0), Control (0)]	**P-Value**	**Adjusted P-Value**	**Fold Enrichment**	**Enrichment Direction**
1 - PS	0.00074	0.02007	9.45	Over
1.5 - PS.carbon concentrating mechanism	0.00128	0.02007	37.35	Over
1.5.1 - PS.carbon concentrating mechanism.C4	0.00128	0.02007	37.35	Over
MapMan BIN codes Group4 [10-OPEA (++), 12-OPDA (+), Control (0)]	**P-Value**	**Adjusted P-Value**	**Fold Enrichment**	**Enrichment Direction**
20.2.1 - stress.abiotic.heat	1.81E-25	9.21E-24	28.14	Over
20.2 - stress.abiotic	6.52E-21	1.66E-19	17.13	Over
20 - stress	8.73E-19	1.48E-17	12.24	Over
26.9 - misc.glutathione S transferases	1.65E-05	0.00021	25.89	Over
29 - protein	0.00142	0.01453	0.20	Under
35 - not assigned	0.00434	0.03166	0.60	Under
35.2 - not assigned.unknown	0.00434	0.03166	0.60	Under
MapMan BIN codes Group5 [10-OPEA (-), 12-OPDA (--), Control (0)]	**P-Value**	**Adjusted P-Value**	**Fold Enrichment**	**Enrichment Direction**
27.3.2 - RNA.regulation of transcription.Alfin-like	3.53E-06	0.00040	36.48	Over
27 - RNA	0.00048	0.02689	1.82	Over
MapMan BIN codes Group6 [10-OPEA (0), 12-OPDA (-), Control (0)]	**P-Value**	**Adjusted P-Value**	**Fold Enrichment**	**Enrichment Direction**
29.2 - protein.synthesis	1.25E-13	2.84E-11	3.48	Over
29.2.1 - protein.synthesis.ribosomal protein	1.55E-09	1.76E-07	3.38	Over
27 - RNA	5.29E-09	4.00E-07	1.78	Over
29.2.1.2.2 - protein.synthesis.ribosomal protein.eukaryotic.60S subunit	2.83E-08	1.61E-06	4.60	Over
29.2.1.2 - protein.synthesis.ribosomal protein.eukaryotic	3.91E-07	1.78E-05	3.33	Over
28 - DNA	4.54E-05	0.00172	2.68	Over
27.3 - RNA.regulation of transcription	0.00015	0.00479	1.55	Over
27.1 - RNA.processing	0.00027	0.00754	2.56	Over
29.2.2.50 - protein.synthesis.misc ribosomal protein.BRIX	0.00037	0.00922	18.90	Over
29.2.1.1 - protein.synthesis.ribosomal protein.prokaryotic	0.00041	0.00922	3.89	Over
27.4 - RNA.RNA binding	0.00045	0.00922	2.74	Over
17.1.1.1 - hormone metabolism.abscisic acid.synthesis-degradation.synthesis	0.00058	0.01094	16.54	Over
28.1 - DNA.synthesis/chromatin structure	0.00104	0.01808	2.62	Over
29.2.1.1.1.2.19 - protein.synthesis.ribosomal protein.prokaryotic.chloroplast.50S subunit.L19	0.00150	0.02439	29.40	Over
29 - protein	0.00162	0.02447	1.30	Over
29.6 - protein.folding	0.00205	0.02903	3.76	Over
17.1.1.1.10 - hormone metabolism.ABA.synthesis-degradation.synthesis.9-cis-epoxycarotenoid dioxygenase	0.00294	0.03513	22.05	Over
29.2.1.2.2.19 - protein.synthesis.ribosomal protein.eukaryotic.60S subunit.L19	0.00294	0.03513	22.05	Over
29.2.6 - protein.synthesis.ribosomal RNA	0.00294	0.03513	22.05	Over
27.3.99 - RNA.regulation of transcription.unclassified	0.00377	0.04280	2.14	Over
29.2.2 - protein.synthesis.misc ribosomal protein	0.00401	0.04332	8.82	Over
27.3.2 - RNA.regulation of transcription.Alfin-like	0.00482	0.04974	8.27	Over
MapMan BIN codes Group7 [10-OPEA (+), 12-OPDA (0), Control (0)]	**P-Value**	**Adjusted P-Value**	**Fold Enrichment**	**Enrichment Direction**
34.99 - transport.misc	0.00011	0.01200	7.81	Over
26.10 - misc.cytochrome P450	0.00038	0.02077	7.95	Over
26 - misc	0.00126	0.04580	2.53	Over
MapMan BIN codes Group8 [10-OPEA (+), 12-OPDA (+), Control (0)]	**P-Value**	**Adjusted P-Value**	**Fold Enrichment**	**Enrichment Direction**
26 - misc	1.35E-18	6.45E-16	2.05	Over
35 - not assigned	2.79E-16	4.43E-14	0.77	Under
35.2 - not assigned.unknown	2.79E-16	4.43E-14	0.77	Under
20 - stress	1.91E-13	2.28E-11	2.08	Over
20.2 - stress.abiotic	5.59E-13	5.34E-11	2.32	Over
20.2.1 - stress.abiotic.heat	8.26E-12	6.57E-10	2.65	Over
29.2 - protein.synthesis	6.70E-11	4.57E-09	0.28	Under
29.2.1 - protein.synthesis.ribosomal protein	1.22E-10	7.25E-09	0.18	Under
26.9 - misc.glutathione S transferases	1.46E-10	7.75E-09	4.88	Over
16.2 - secondary metabolism.phenylpropanoids	4.49E-09	2.14E-07	3.43	Over

Table S2: MapMan categorical enrichment (continued)				
MapMan BIN codes Group8 [10-OPEA (+), 12-OPDA (+), Control (0)] (continued)	P-Value	Adjusted P-Value	Fold Enrichment	Enrichment Direction
34 - transport	2.43E-08	1.05E-06	1.62	Over
26.2 - misc.UDP glucosyl and glucoronyl transferases	3.11E-08	1.23E-06	2.64	Over
29.2.1.2 - protein.synthesis.ribosomal protein.eukaryotic	3.62E-08	1.33E-06	0.18	Under
16.2.1 - secondary metabolism.phenylpropanoids.lignin biosynthesis	1.57E-07	5.36E-06	4.13	Over
16 - secondary metabolism	6.65E-07	2.11E-05	2.04	Over
27 - RNA	1.16E-06	3.45E-05	0.73	Under
26.10 - misc.cytochrome P450	5.01E-06	0.00014	2.65	Over
28 - DNA	6.55E-06	0.00017	0.33	Under
29 - protein	1.04E-05	0.00026	0.80	Under
17.7.1 - hormone metabolism.jasmonate.synthesis-degradation	2.06E-05	0.00049	4.55	Over
27.1 - RNA.processing	6.66E-05	0.00145	0.37	Under
17.7 - hormone metabolism.jasmonate	6.67E-05	0.00145	4.05	Over
34.8 - transport.metabolite transporters at the envelope membrane	8.13E-05	0.00169	4.86	Over
29.2.1.2.1 - protein.synthesis.ribosomal protein.eukaryotic.40S subunit	8.97E-05	0.00178	0.09	Under
27.3.32 - RNA.regulation of transcription.WRKY domain transcription factor family	0.00010	0.00192	3.00	Over
28.1 - DNA.synthesis/chromatin structure	0.00010	0.00192	0.30	Under
29.2.1.2.2 - protein.synthesis.ribosomal protein.eukaryotic.60S subunit	0.00011	0.00199	0.24	Under
27.3.67 - RNA.regulation of transcription.putative transcription regulator	0.00012	0.00207	0.24	Under
11.8.1 - lipid metabolism.exotics (steroids, squalene etc).sphingolipids	0.00015	0.00253	3.44	Over
1.1 - PS.lightreaction	0.00022	0.00357	0.21	Under
16.2.1.10 - secondary metabolism.phenylpropanoids.lignin biosynthesis.CAD	0.00027	0.00412	6.83	Over
34.99 - transport.misc	0.00034	0.00506	2.08	Over
30.3 - signalling.calcium	0.00049	0.00707	1.82	Over
17.7.1.2 - hormone metabolism.jasmonate.synthesis-degradation.lipoxygenase	0.00055	0.00768	6.07	Over
29.2.1.1 - protein.synthesis.ribosomal protein.prokaryotic	0.00056	0.00769	0.11	Under
31.4 - cell.vesicle transport	0.00060	0.00793	1.84	Over
11.8.1.2 - lipid metabolism.exotics (steroids, squalene etc).sphingolipids.serine C-palmitoyltransferase	0.00076	0.00959	10.93	Over
10.5.5 - cell wall.cell wall proteins.RGP	0.00076	0.00959	10.93	Over
4.1.14 - glycolysis.cytosolic branch.pyruvate kinase (PK)	0.00086	0.01058	7.29	Over
26.1 - misc.misc2	0.00099	0.01179	2.80	Over
17 - hormone metabolism	0.00109	0.01258	1.54	Over
29.5 - protein.degradation	0.00111	0.01258	0.77	Under
10.1 - cell wall.precursor synthesis	0.00127	0.01414	2.57	Over
30 - signalling	0.00146	0.01579	1.28	Over
17.7.1.5 - hormone metabolism.jasmonate.synthesis-degradation.12-Oxo-PDA-reductase	0.00183	0.01785	6.25	Over
13.1.5.1 - amino acid metabolism.synthesis.serine-glycine-cysteine group.serine	0.00183	0.01785	6.25	Over
13.1.6.3 - amino acid metabolism.synthesis.aromatic aa.phenylalanine	0.00183	0.01785	6.25	Over
34.19.3 - transport.Major Intrinsic Proteins.NIP	0.00183	0.01785	6.25	Over
1.2.5 - PS.photorespiration.serine hydroxymethyltransferase	0.00183	0.01785	6.25	Over
29.3.4.99 - protein.targeting.secretory pathway.unspecified	0.00203	0.01940	2.33	Over
29.5.11.20 - protein.degradation.ubiquitin.proteasom	0.00223	0.02082	0.13	Under
27.3.27 - RNA.regulation of transcription.NAC domain transcription factor family	0.00233	0.02135	2.67	Over
4.1 - glycolysis.cytosolic branch	0.00241	0.02169	2.51	Over
29.3.4 - protein.targeting.secretory pathway	0.00259	0.02284	1.77	Over
34.16 - transport.ABC transporters and multidrug resistance systems	0.00277	0.02362	2.03	Over
27.3 - RNA.regulation of transcription	0.00277	0.02362	0.84	Under
2.2.1 - major CHO metabolism.degradation.sucrose	0.00314	0.02629	2.73	Over
27.4 - RNA.RNA binding	0.00327	0.02686	0.49	Under
10.1.5 - cell wall.precursor synthesis.UXS	0.00333	0.02694	5.47	Over
21.2.2 - redox.ascorbate and glutathione.glutathione	0.00381	0.03032	4.20	Over
27.3.3 - RNA.regulation of transcription.AP2/EREBP, APETALA2/Ethylene-responsive element binding protein family	0.00476	0.03719	2.19	Over
11.8 - lipid metabolism.exotics (steroids, squalene etc)	0.00498	0.03830	2.09	Over
34.19.2 - transport.Major Intrinsic Proteins.TIP	0.00545	0.04065	4.86	Over
30.2 - signalling.receptor kinases	0.00545	0.04065	1.49	Over
16.1.5 - secondary metabolism.isoprenoids.terpenoids	0.00591	0.04244	3.28	Over
20.2.2 - stress.abiotic.cold	0.00591	0.04244	3.28	Over
31.1 - cell.organisation	0.00596	0.04244	0.59	Under
13.1.5.1.1 - amino acid metabolism.synthesis.serine-glycine-cysteine group.serine.phosphoglycerate dehydrogenase	0.00631	0.04302	6.56	Over
26.11.1 - NA	0.00631	0.04302	6.56	Over
20.1 - stress.biotic	0.00631	0.04302	1.59	Over
30.2.17 - signalling.receptor kinases.DUF 26	0.00684	0.04595	1.88	Over
26.22 - misc.short chain dehydrogenase/reductase (SDR)	0.00725	0.04802	2.40	Over
17.5.2 - hormone metabolism.ethylene.signal transduction	0.00751	0.04909	3.12	Over

Table S2: MapMan categorical enrichment (continued)				
MapMan BIN codes Group9 [10-OPEA (-), 12-OPDA (-), Control (0)]	P-Value	Adjusted P-Value	Fold Enrichment	Enrichment Direction
29.5.5 - protein.degradation.serine protease	7.23E-06	0.00352	2.92	Over
29.2.1.2 - protein.synthesis.ribosomal protein.eukaryotic	2.00E-05	0.00487	0.31	Under
16.1.4 - secondary metabolism.isoprenoids.carotenoids	0.00010	0.01687	4.79	Over
1.1.5 - PS.lightreaction.other electron carrier (ox/red)	0.00019	0.02021	3.99	Over
1.1.5.3 - PS.lightreaction.other electron carrier (ox/red).ferredoxin reductase	0.00022	0.02021	9.57	Over
1.1 - PS.lightreaction	0.00025	0.02021	2.02	Over
29.2.5 - protein.synthesis.release	0.00032	0.02192	5.52	Over
29.2.1.2.2 - protein.synthesis.ribosomal protein.eukaryotic.60S subunit	0.00037	0.02253	0.26	Under
1 - PS	0.00061	0.02606	1.71	Over
18.5.2 - Co-factor and vitamine metabolism.folate & vitamine K.vitamine K	0.00061	0.02606	7.98	Over
35 - not assigned	0.00064	0.02606	1.08	Over
35.2 - not assigned.unknown	0.00064	0.02606	1.08	Over
26.2 - misc.UDP glucosyl and glucoronyl transferases	0.00089	0.03245	0.24	Under
20 - stress	0.00094	0.03245	0.61	Under
29.3.3 - protein.targeting.chloroplast	0.00103	0.03245	2.80	Over
27.3.60 - RNA.regulation of transcription.NIN-like bZIP-related family	0.00111	0.03245	5.44	Over
29.1.30 - protein.aa activation.pseudouridylate synthase	0.00113	0.03245	4.49	Over
13.1.1.3.11 - amino acid metabolism.synthesis.central AA metabolism.alanine.alanine-glyoxylate aminotransferase	0.00131	0.03544	6.84	Over
29.2.1 - protein.synthesis.ribosomal protein	0.00145	0.03709	0.57	Under

Supplemental Table S3. Primer pairs used for qRT-PCR expression analysis.

Gene	MaizeGDB ID	Forward Primer Sequence	Reverse Primer Sequence	Amplicon	Efficiency (%)	R^2
PR4b	GRMZM2G117971	ATGGATGTGATCCCACACG	TCGTGAGACATGACGATAC	103 bp	92	0.982
OPR2	GRMZM2G000236	GACCGACCGAGAGCAAATAG	ATCTTGTAAGGCGTCAGCAG	92 bp	108	0.985
CCD1	AC225718.2_FG006	TAGCTGGATGGATCAGGACTT	ATTGGAACATGGGAATTGGG	96 bp	105	0.994
GST2	GRMZM2G132093	TGTGCTTGATTAGTTAATTGG	CGTGGAGAAAGCAGCAAAAT	101 bp	98	0.997
HYD	GRMZM2G159477	TGTGCCAGGTGCTTGCGTT	TGAAAGCAGGATAAACACCAA	111 bp	100	0.991
OXR	GRMZM2G020631	TGATGTTTGGTACAGAGTG	TCATCCCGTCAGAGGTTTTA	94 bp	96	0.997
WIP1	GRMZM2G156632	GTCCGAGACCATGAAGAGC	AGGAGAAGTTGCAGTTGGTG	170 bp	Huffaker et al., 2013 (1)	
SerPIN	GRMZM5G815098	GACCTCAGGCGTCGTTACTC	TGCAGCAAATATAGCCAACG	105 bp	Erb et al., 2009 (2)	
ZmCC9	AC196110.4_FG004	GATCATCCCGTAGCCATCTG	CACTGTTCCATGCCACTGAC	134 bp	van der Linde et al., 2012 (3)	
LOX1	GRMZM2G156861	TCTGTCTGAGCTGAGGACGTA	CACAAAGTAACTTCATTATTGAGGA	186 bp	Vaughan et al., 2014 (4)	
LOX2	GRMZM2G156861	TTCCATCTGATTCGATCGAG	CACATTATTATTGGGAAACCAAC	230 bp	Vaughan et al., 2014 (4)	
LOX3	GRMZM2G109130	TACCACTACCACCCCAGGAGT	AGCACTGCGAAACGACTAGAA	233 bp	Vaughan et al., 2014 (4)	
LOX4	GRMZM2G109056	TGAGCGGATGGTTTGTAGAT	ATTATCCAGACGTGGCTCCT	170 bp	Vaughan et al., 2014 (4)	
LOX5	GRMZM2G102760	GGGCAGATTGTGTCTCGTAGTA	ATATTCAAGCGTGGACTCCTCT	140 bp	Vaughan et al., 2014 (4)	
LOX6	GRMZM2G040095	ACAGCCCTGACTGGTGCTC	TTCACGTTTATGTGGTGGAGA	172 bp	Vaughan et al., 2014 (4)	
LOX8	GRMZM2G104843	CAGTACCGACAGACAGCCAT	GTTTCGGACCACCAAATCAA	163 bp	Vaughan et al., 2014 (4)	
LOX9	GRMZM2G017616	TGAGTGCATCGTTCGTTGT	TCAATCCTCATTCTTGGCAG	152 bp	Vaughan et al., 2014 (4)	
LOX10	GRMZM2G015419	ATCCTCAGCATGCATTAGTCC	AGTCTCAAACGTGCCTCTTGT	139 pb	Vaughan et al., 2014 (4)	
LOX11	GRMZM2G009479	GTCCGTCCTCTCCATCCAA	GGATCTGCTAGTAATGTCATCC	191 bp	Vaughan et al., 2014 (4)	
LOX12	GRMZM2G106748	AATTGACAAGCTCGCTCCTT	TCCAAACCAATCATCGCAA	124 bp	Vaughan et al., 2014 (4)	
AOS1	GRMZM2G067225	ACAAGGTGGAGAAGAAGGAC	GTCGTTGAGCTTGTTGAACT	257 bp	Huffaker et al., 2013 (1)	
AOS2	GRMZM2G072653	TCTATGTAAAATGGCCTGGGA	ATAATTTGCGAGCCCATCCG	100 bp	133	0.949
AOS3	GRMZM2G376661	GTACTGACACGCTCGCCTTA	ACAGCGAGTGACGTGTGCA	66 bp	93	0.981
PR1	GRMZM2G465226	GAGAACTCGCCTCAAGACTAC	GGCGTATTTGTACCACTGTTT	255 bp	Doehlmann et al., 2008 (5)	
PR5	GRMZM2G402631	TCTACGACATCTCGGTCATC	GACTTGGTAGTTGCTGTTGC	161bp	93	0.964
PRM6b	GRMZM2G065585	CATCTTCGCCATGTTCAACG	ATTTGTCCGGGTTGAAGAGG	80 bp	van der Linde et al., 2012 (3)	
P450	GRMZM2G129860	CTGACCGCATATGTAGAAA	TCGCAATGCATACAAGGGA	109 bp	92	0.921
UBCP*	GRMZM2G102471	CAGGTGGGGTATTCTTGGTG	ATGTTCGGGTGGAAAACCTT	231 bp	Manoli et al., 2012 (6)	
FPGS*	GRMZM2G393334	ATCTCGTTGGGGATGTCTTG	AGCACCGTTCAAATGTCTCC	132 bp	Manoli et al., 2012 (6)	

*Reference genes used for quantitative transcript analysis

1. Huffaker A, et al. (2013) Plant elicitor peptides are conserved signals regulating direct and indirect antiherbivore defense. *Proc Natl Acad Sci USA* 110(14):5707-5712.

2. Erb M, et al. (2009) Signal signature of aboveground-induced resistance upon belowground herbivory in maize. *Plant J* 59(2):292–302.

3. van der Linde K, et al. (2012) A maize cystatin suppresses host immunity by inhibiting apoplastic cysteine proteases. *Plant Cell* 24(3):1285-1300.

4. Vaughan MM, et al. (2014) Effects of elevated [CO2] on maize defense against mycotoxigenic *Fusarium verticillioides*. *Plant Cell & Environ* 37(12): 2691-2706.

5. Doehlemann G, et al. (2008) Reprogramming a maize plant: transcriptional and metabolic changes induced by the fungal biotroph *Ustilago maydis*. *Plant J* 56(2):181–195.

6. Manoli A, Sturaro A, Trevisan S, Quaggiotti S, Nonis A (2012) Evaluation of candidate reference genes for qPCR in maize. *J Plant Physiol* 169(8):807–8150.